

# A NEW MATHEMATICAL MODEL FOR CELL MOTILITY WITH NONLOCAL REPULSION FROM SATURATED AREAS

CARLO GIAMBIAGI FERRARI, FRANCISCO GUILLÉN-GONZÁLEZ, MAYTE PÉREZ-LLANOS,  
AND ANTONIO SUÁREZ

**ABSTRACT.** The main purpose of this work is the mathematical modelling of large populations of cells under different deterministic interactions among themselves, in balance with naturally random diffusion. We focus on cell-cell adhesion mechanisms for a single population confined to an isolated domain. Our most relevant contribution is to derive a mathematical model including a nonlocal saturation coefficient as part of an appropriate nonlocal drift term, including repulsion effects, depending on the level of saturation of the area. For this purpose, we use two discrete approaches taking into account different perspectives: Eulerian and Lagrangian reference systems.

## 1. INTRODUCTION

Cellular movements are critical for a wide number of biological processes, including normal embryogenesis, tissue formation, wound healing and even defense against infection, among others. It is also an important factor in diseases such as cancer metastasis and birth defects. It is well known that cell interaction involves attraction and repulsion. Cells need to be sufficiently close to attract each other. At the same time, they also exhibit certain random movement. The overall evolution is a result of the balance between the diffusion originated from the Brownian motion and the transport due to deterministic interactions. For instance, see [4] and [6] for a general description on cell motion. Cells might move attracted by other cells. However, as an area becomes too crowded, the attraction weakens as other cells tend to less populated areas and a repulsion effect appears. This way high accumulations at narrow zones or single points are prevented from occurring.

In the last decade, introducing non-local terms in the classical PDEs governing many of the biological processes is an issue that is increasingly employed, see for example [21]. The process of gaining information about presence or absence of other species in the environment is intrinsically non-local, be it higher level species or cells. Animals explore their surroundings to find prey, avoid predators or aggregate in colonies, herds or swarms, (we refer to e.g. [10], [15], [23], [24]). This non-local sensing, which in animals is due mainly to using smell, hearing or sight, it also occurs at cellular level, through the extension of long thin protrusions, see [30].

In mathematical modelling on the population level, non-local integro-differential operators allow to capture the drift motion caused by interactions between cells more accurately than local differential operators. This is due to their ability to take into account the effect of the surrounding environment to describe what happens at certain point, in contrast to local differential operators. A recent review on this topic is [22]. In this respect one pioneer reference is the work [2], where a non-local equation was adopted for the first time in the context of cell-cell adhesion modelling. There, the velocity of the drift due to adhesion is defined so that its motion is described by an integral operator. Moreover, the authors point out the ability of the model to replicate fundamental behaviour associated with cell-cell adhesion and the active sorting process of two or more cell types from a randomly distributed mixture.

---

*Key words and phrases.* Nonlocal gradient, random diffusion, nonlocal saturation coefficient, confined dynamics  
2000 *Mathematics Subject Classification* 92C17, 92C37, 35Q92 .

This model inspired a large number of subsequent contributions, including [12], [25], [26], [31], see also the review [13] and references therein.

According to the previous short overview on mathematical modelling of cell-to-cell interactions, non-locality in continuum models often arises as an integral term inside a derivative. Consequently, many of the mathematical techniques developed to deal with classical PDEs (such as comparison and monotonicity methods, spectral theory, Lyapunov functionals, etc) need to be adapted or even redefined appropriately to apply them within this non-local framework, we refer for instance to [29], [7], [9]. However, it is not always possible to find suitable arguments based on classical theories, which gives rise to new challenging directions of work within the analysis of PDEs. As a counterpart, in single-population models of aggregation, the nonlocal structure of the advective term is fundamental to avoiding blow-up phenomena, that is, unbounded solutions at finite time, and ensuring global existence, [9], [14], [16], [17] or [19], among others.

The primary focus of this work is to describe large populations of cells: how do they evolve in confinement when interaction among them is driven by attraction and avoidance of too saturated areas. Moreover, we determine adequate microscopic rules specifically regulating different mechanisms of attraction or repulsion, evaluating the effect of each parameter or term in those relations and their impact on the underlying macroscopic behavior.

The content of this paper is organized as follows: We begin by summarizing in Section 2, some existing literature that is a starting point of our work. In Section 3 we propose several discrete models inspired by some of the references mentioned in Section 2, thereby adopting the Eulerian perspective. Namely, defining an initial (discrete) density of  $N$  cells, we determine its changing rate at every time step, as a balance between loss and gain terms, resulting from different deterministic rules in combination with random motion. This analysis will relate our models as  $N \rightarrow \infty$  with certain PDEs containing nonlocal terms. In Section 4 this study will be complemented with a Lagrangian formulation, where we focus on the motion of individual cells, according to the mentioned rules. This leads to a system of  $N$  SDEs describing the cell trajectories. As it could be expected, in the hydrodynamic limit as  $N \rightarrow \infty$  this system recovers nonlocal PDEs. However, both points of view are useful. On the one side, Lagrangian perspective allows us to follow every single cell, which is not possible when dealing with densities in the eulerian perspective. On the other side however, the trajectory simulations correspond to a reduced number of particles, thus saturation effects are better described by the PDEs eulerian approach. At this point, the discrete eulerian modelling could be viewed as a numerical discretization of such PDEs. Nevertheless, due to the intricate nature of the problem we use appropriate semi-explicit upwind schemes instead, to obtain reliable results when representing numerical simulations in Section 5. Several observations for different interactions will be illustrated by a variety of examples, based on both, Lagrangian trajectories and PDEs discretizations. We conclude the paper with the main conclusions of our analysis in Section 6.

## 2. OVERVIEW OF RELATED CELL-CELL ADHESION MODELS

We begin briefly reviewing the Armstrong Painter Sherratt 1D model (APS model), from [2], where the density of a population of cells  $u = u(x, t) \geq 0$  evolves in a spatial 1D domain  $x \in \Omega = (-L, L)$  during a time interval  $t \in [0, +\infty)$  according to the nonlocal PDE

$$(2.1) \quad u_t(x, t) = u_{xx}(x, t) - \gamma \partial_x \left( u(x, t) K(u)(x, t) \right),$$

where

$$(2.2) \quad K(u)(x, t) = \int_0^R (g(u(x+r, t)) - g(u(x-r, t)))\omega(r)dr.$$

Here,  $\gamma > 0$  is a parameter representing the strength of the adhesion with respect to the diffusion. The function  $g(u(x+r, t))$  and  $g(u(x-r, t))$  describes the dependence of the local force acting on the cell at position  $x$  due to the cells at position  $x+r$  or  $x-r$ . The weight  $\omega(r)$  modifies the previous force according to the distance  $r$  between the cells. The total force acting on the cell at position  $x$  is given by  $\gamma K(u)(x, t)$ . This global force accounts only for the action of the cells at distance from  $x$  less than the sensing radius  $R > 0$ . Namely,  $\omega(r) = 0$  for  $r > R$  is imposed.

The main novelty of [2] resides in the proposed adhesion term  $\partial_x(u(x, t)K(u)(x, t))$ , where  $K(u)(x, t)$  is the drift nonlocal term given in (2.2). The authors simplify the model by taking  $g(u) = u$  and  $\omega \equiv 1$  in  $[0, R]$ , though warned that a non-constant function would be more realistic. In this case, the integral term  $K(u)(x, t)$  moves the cells towards more populated areas, giving raise to strong aggregation in several peaks, separated by  $2R$  distance. In these examples periodic boundary conditions were considered by convenience. Further simulations are presented in [2], taking  $\omega \equiv 1$  in  $[0, R]$  and  $g(u) = u(1 - u/K)_+$ , which is truncated at the crowding capacity  $K > 0$ . This modification ensures that cells travel to moderately populated areas, softening the above mentioned peaks. In addition [2] also contains a study of several kinds of interactions between two populations of different type of cells in the two dimensional setting, which is out of the scope of the present work.

Murakawa and Togashi found in [25] that, when extended to two cell types, the APS model was unable to replicate properly certain cell sorting patterns observed experimentally. Adopting a logistic function for  $g(u)$ , they proposed to replace the linear laplacian diffusion by a porous media diffusion, obtaining a model that captures more accurately the behaviour the authors expected, according to experimental results. Note that already in the case of a single population, this nonlinear porous media diffusion introduces intrinsically a repulsion effect from more crowded areas to empty spaces, that is stronger than in the Laplacian case, where diffusivity is uniform across the domain. To avoid cells drifting to medium populated areas, as it happens in [25], the following modification of the drift velocity was proposed in [12]

$$K(u)(x, t) = (1 - u(x, t)) \int_0^R (u(x+r, t) - u(x-r, t))\omega(r)dr,$$

where the crowding capacity has been rescaled to  $K = 1$ . In fact, the variable  $u$  in this model can be interpreted as the volume fraction of cells, since it doesn't exceed one if the initial values are below one as well. Solutions of the model in [12] behave differently to those of the APS model. On the one hand, even though cells are directed to most populated areas by the non-local integral term, the velocity of their movement is multiplied by the factor  $(1 - u(x, t))$ . This velocity is slower as the density of cells reaches gradually higher values at point  $x$ . Therefore, this coefficient slows down cells motion according to the local crowdedness of the model at each  $x$ . On the other hand, the nonlinear diffusion of porous media type also considered in [12] introduces a repulsion effect to further avoid accumulating in high crowded areas.

We notice that repulsion due to saturation is absent in the original APS model, while in [12] and [25] it is driven by the nonlinear diffusion of porous media type, and not by the drift term. Some remarks in [12] admit that the weight  $\omega(r)$  needs to take positive (aggregation) and negative (repulsion) values, depending on the distance among the interacting cells. See also [20], where an intercellular interaction kernel introduces change of sign of parabolic shape. Therefore, this kernel defines short, middle and long range interactions. However, it is not taken into account that the saturation of the area should also lead to repulsion. The main aims of this paper is to explore the dynamics including repulsion by

saturation as part of the drift term. In this respect the choice of the weight will contribute to regulate the effect of repulsion or aggregation.

Although [2], [12] and much of the existing literature on mathematical modelling of cell-cell adhesion consider periodic boundary conditions, with the consequent simplification of the simulation codes, this approach is just appropriate whenever the size of the domain can be considered infinitely large with respect to cells size. Nevertheless, it is also relevant the study of single-cell migrating in isolation medium. The work [18] introduces several models in bounded domains considering either adhesive, or repulsive or even neutral boundary effects. Moreover, some numerical simulations are included illustrating the different boundary effects.

In the above description, we have limited ourselves to summarizing the models that have mainly inspired our work. Nevertheless, as we already mentioned, there exists a wide variety of contributions based on the APS model due to Armstrong, Painter and Sherrat, see the book [7] and references therein.

Summarizing, the main novelty of our modelling is that it captures more accurately the repulsion from saturated areas by a nonlocal factor included in an appropriate nonlocal drift term in isolated domains.

### 3. EULER PERSPECTIVE

In this Section we develop various discrete models under the Euler perspective. We use the approach similar to [27] (see also [1] for a similar modelling approach to a biological application). For simplicity, we work in a one-dimensional space and consider a domain  $\Omega = (-L, L)$ . The extension to higher dimensions is straightforward, but would cause high computational cost in the subsequent simulations.

We construct models in which the unknown variable is the proportion of cells at certain position, combining infinitesimal motion directed by a nonlocal signal depending on the nonlocal term given in (2.2) with random diffusive processes.

**3.1. Generic balance.** Consider a population of  $N \in \mathbb{N}$  cells that we enumerate from 1 to  $N$ . At time  $t \geq 0$  we assign a real number  $x_i(t) \in \bar{\Omega} = [-L, L]$ , representing the position of the cell number  $i \in \{1, \dots, N\}$ . The cell's position can only change due to a diffusion process and different nonlocal interactions with other cells, that are at a distance smaller than a sensing radius  $R > 0$ .

In order to obtain master equations, let us subdivide the interval  $[-L, L]$  in a family of intervals  $\{I_j\}, j \in \{1, \dots, M\}$  of equal length  $h = 2L/M$ . In the sequel, it will be convenient to declare as  $y_j$  the midpoint of the interval  $I_j$ . For  $t \geq 0$ , we denote by

$$s_j(t) = \frac{\#\{i : x_i(t) \in I_j\}}{N}$$

the proportion of cells with position within the interval  $I_j$  at time  $t$ . Obviously,  $\sum_{j=1}^M s_j(t) = 1$  for all  $t \geq 0$ .

As in [27], we want to derive a system of  $M$  recursive discrete equations based on the assumption that the proportion of cells at the interval  $I_j$  at stage  $t + \Delta t$ , namely  $s_j(t + \Delta t)$ , equals the proportion of cells at  $I_j$  in the previous stage  $s_j(t)$ , plus certain gain and loss terms, representing the changes as cells enter and leave  $I_j$ , respectively, under the action of intercell interactions and diffusion. Obviously, the magnitude of these gain and loss terms depend on how long we consider the time step  $\Delta t$  to be. At this point we stress an important difference with respect to [27]. In our model, the gain and loss terms result from two different effects, interactions and diffusion, which do not occur necessarily with the same frequency. The detailed analysis below shows that indeed, each of these processes has its own

scale. Let us fix the characteristic time step  $\Delta t$ . Then,

$$(3.1) \quad s_j(t + \Delta t) = s_j(t) + \Delta t \left[ Q_{\text{diff}}^h \left( G_{\text{diff}}(j, t) - L_{\text{diff}}(j, t) \right) + Q_{\text{int}}^h \left( G_{\text{int}}(j, t) - L_{\text{int}}(j, t) \right) \right],$$

for  $j \in \{1, \dots, M\}$ , where  $G_{\text{diff}}(j, t)$  and  $G_{\text{int}}(j, t)$  stand for probability gain rates while  $L_{\text{diff}}(j, t)$  and  $L_{\text{int}}(j, t)$  represent loss rates, corresponding to diffusion and interaction effects, respectively. The coefficients  $Q_{\text{diff}}^h$  and  $Q_{\text{int}}^h$  account for the frequency of diffusion and interaction processes, respectively, per unit of time. The key to assemble correctly these two mechanisms of motion is precisely the determination of the exact dependence on  $h$  of coefficients  $Q_{\text{diff}}^h$  and  $Q_{\text{int}}^h$ .

The study of the resulting system of  $M$  equations (for  $M$  large) is easier if considering its reformulation for probability density. To this end, we introduce a piecewise constant in space function  $u_h$ , representing a discrete probability density of the cell population, namely

$$(3.2) \quad u_h(y, t) : [-L, L] \times [0, \infty) \rightarrow \mathbb{R}_0^+ \quad \text{such that } (u_h(\cdot, t))|_{I_j} = s_j(t)/h.$$

In particular,  $s_j(t) = \int_{I_j} u_h(y, t) dy$ .

From now on we focus on the system of equations (3.1) and rewrite it in terms of the function  $u_h$ . Assuming that there is a limit function  $u(x, t)$  such that  $u_h \rightarrow u$  as  $h \rightarrow 0$  in some sense and also that  $(u_h(\cdot, t))|_{I_j}$  is bounded as  $h$  goes to zero, our aim is to determine (formally) which are the different PDEs satisfied by  $u$ , depending on the model under consideration. Notice that for example,  $u_h$  could be regarded as an appropriate numerical approximation of  $u$ .

**3.2. Motion due to aggregation through nonlocal terms [2].** We begin our study with the simplest case of the APS model given in [2], for which the direction of the transport term is determined by nonlocal terms depending on the density of cells. The action of the surrounding cells could be neglected beyond certain threshold,  $R > 0$ , known as the *sensing cell radius*. Moreover, this action could also decrease with respect to the distance between the interacting cells, through a weight  $w = w(r)$  with

$$(3.3) \quad w : [0, +\infty) \rightarrow \mathbb{R}_0^+ \quad \text{such that } w(r) > 0 \text{ if } r \in [0, R) \text{ whereas } w(r) = 0 \text{ if } r \geq R.$$

Interaction forces between cells belonging to  $I_i$  and  $I_j$ , respectively, will be weighted by  $w(|y_j - y_i|)$  being  $y_k$  the midpoint of each  $I_k$ . This model corresponds to the following gain and loss terms: the proportion of cells arriving to  $I_j$  and leaving  $I_j$  are, respectively

$$\begin{aligned} G_{\text{int}}(j, t) &= s_{j+1}(t)P_{I_{j+1} \rightarrow I_j}(t) + s_{j-1}(t)P_{I_{j-1} \rightarrow I_j}(t), \\ L_{\text{int}}(j, t) &= s_j(t) \left[ P_{I_j \rightarrow I_{j-1}}(t) + P_{I_j \rightarrow I_{j+1}}(t) \right]. \end{aligned}$$

Notice that space motion is considered to be local, because the arriving cells to interval  $I_j$  come just from the adjacent positions,  $I_{j-1}$ ,  $I_{j+1}$ . On the other hand, the cells leaving  $I_j$  can just move to either  $I_{j-1}$  or  $I_{j+1}$ .

In contrast, the transition probabilities are nonlocal. They depend on the neighbouring configuration of the population inside the sensing radius  $R$  from interval  $I_j$ . Namely, related to the gain term

$$(3.4) \quad P_{I_{j+1} \rightarrow I_j}(t) = \sum_{i=j-r}^j s_i(t)w(y_{j+1} - y_i), \quad P_{I_{j-1} \rightarrow I_j}(t) = \sum_{i=j}^{j+r} s_i(t)w(y_i - y_{j-1}),$$

and similarly, regarding the loss term,

$$P_{I_j \rightarrow I_{j-1}}(t) = \sum_{i=j-1-r}^{j-1} s_i(t)w(y_j - y_i) \quad P_{I_j \rightarrow I_{j+1}}(t) = \sum_{i=j+1}^{j+1+r} s_i(t)w(y_i - y_j).$$

Here, the natural number  $r$  is in fact  $r = r(h)$ , such that  $r(h) = [R/h]$ , where  $[x]$  denotes the integer part of  $x$ . To shorten the notation, we introduce the following terms

$$\text{Left}(j, t) := s_{j+1}(t)P_{I_{j+1} \rightarrow I_j}(t) - s_j(t)P_{I_j \rightarrow I_{j-1}}(t),$$

$$\text{Right}(j, t) := s_{j-1}(t)P_{I_{j-1} \rightarrow I_j}(t) - s_j(t)P_{I_j \rightarrow I_{j+1}}(t),$$

hence

$$(3.5) \quad G_{\text{int}}(j, t) - L_{\text{int}}(j, t) = \text{Left}(j, t) + \text{Right}(j, t).$$

Note that, by the definition (3.2) and assuming that  $w|_{[0, R]} \in C^2([0, R])$ , by the midpoint quadrature rule, and recalling that  $u_h(y_i, t)$  is bounded with respect to  $h$ , one has

$$(3.6) \quad s_i(t)w(|y_{j+1} - y_i|) = \int_{I_i} u_h(y, t)w(|y_{j+1} - y|)dy + O(h^3),$$

hence, from (3.4),

$$P_{I_{j+1} \rightarrow I_j}(t) = \int_{\bigcup_{i=j-r}^j I_i} u_h(y, t)w(y_{j+1} - y)dy + O(h^2).$$

Similarly, one has

$$P_{I_{j-1} \rightarrow I_j}(t) = \int_{\bigcup_{i=j}^{j+r} I_i} u_h(y, t)w(y - y_{j-1})dy + O(h^2).$$

At this point, we define the following operators acting on a generic function  $v$ :

$$\mathcal{G}^- v(x, t) = \int_{x-R}^x v(y, t)w(x - y)dy, \quad \mathcal{G}^+ v(x, t) = \int_x^{x+R} v(y, t)w(y - x)dy,$$

and its discrete version acting on a generic piecewise constant function  $v_h$  on intervals  $I_j$ , for  $j \in \{1, \dots, M\}$ :

$$(3.7) \quad \begin{aligned} \mathcal{G}_h^- v_h(y_{j+1}, t) &:= \int_{\bigcup_{i=j-r}^j I_i} v_h(y, t)w(y_{j+1} - y)dy, \\ \mathcal{G}_h^+ v_h(y_{j-1}, t) &:= \int_{\bigcup_{i=j}^{j+r} I_i} v_h(y, t)w(y - y_{j-1})dy. \end{aligned}$$

One arrives then, recalling that  $u_h(y_j, t)$  is bounded, at

$$\begin{aligned} \text{Left}(j, t) &= \left[ h u_h(y_{j+1}, t) \right] \left[ \mathcal{G}_h^- u_h(y_{j+1}, t) + O(h^2) \right] - \left[ h u_h(y_j, t) \right] \left[ \mathcal{G}_h^- u_h(y_j, t) + O(h^2) \right] \\ &= h^2 \left[ \frac{u_h(y_{j+1}, t)\mathcal{G}_h^- u_h(y_{j+1}, t) - u_h(y_j, t)\mathcal{G}_h^- u_h(y_j, t)}{h} \right] + O(h^3). \end{aligned}$$

Analogously,

$$\text{Right}(j, t) = -h^2 \left[ \frac{u_h(y_j, t)\mathcal{G}_h^+ u_h(y_j, t) - u_h(y_{j-1}, t)\mathcal{G}_h^+ u_h(y_{j-1}, t)}{h} \right] + O(h^3).$$

We combine the left and right terms and denote forward and backward differences with respect to  $y$  variable by

$$(3.8) \quad \partial_h^+ v(y, t) := \frac{v(y+h, t) - v(y, t)}{h}, \quad \text{and} \quad \partial_h^- v(y, t) := \frac{v(y, t) - v(y-h, t)}{h}.$$

Then, according to (3.5), we have shown that

$$(3.9) \quad G_{\text{int}}(t, j) - L_{\text{int}}(t, j) = -h^2 \mathcal{T}_{aps}^h(y_j, t) + O(h^3),$$

where

$$(3.10) \quad \mathcal{T}_{aps}^h(y_j, t) := \partial_h^- \left[ u_h(y_j, t) \mathcal{G}_h^+ u_h(y_j, t) \right] - \partial_h^+ \left[ u_h(y_j, t) \mathcal{G}_h^- u_h(y_j, t) \right].$$

Let  $x \in [-L, L]$  be an arbitrary point. For each uniform partition of length  $h$ , we can choose an index  $j = j(h)$  such that  $y_j \rightarrow x$  as  $h \rightarrow 0$ . In conclusion, assuming that  $u_h \rightarrow u$  as  $h \rightarrow 0$ , the following approximation can be (formally) deduced

$$\lim_{h \rightarrow 0} \mathcal{T}_{aps}^h(y_j, t) = \frac{\partial}{\partial x} \left( u(x, t) (\nabla_{NL} u)(x, t) \right),$$

where the nonlocal term  $\nabla_{NL} u$  is defined as

$$(\nabla_{NL} u)(x, t) := \mathcal{G}^+ u(x, t) - \mathcal{G}^- u(x, t) = \int_x^{x+R} u(y, t) w(y - x) dy - \int_{x-R}^x u(y, t) w(x - y) dy,$$

which can be rewritten as

$$(3.11) \quad (\nabla_{NL} u)(x, t) = \int_0^R (u(x + r, t) - u(x - r, t)) w(r) dr.$$

As observed in Section 2, in [2] it is considered as part of the drift the nonlocal term  $\nabla_{NL} g(u)$  of the truncated logistic function  $g(u) = u(1 - u)_+$ , see (2.2). This choice allows to avoid the strong aggregation observed in the basic APS model, though it does not fit the point of view of our modeling. Note that in case  $g(u) = u(1 - u)_+$ , it is not possible to write the motion as a balance between gain and loss terms. As reviewed earlier in Section 2, in [12] the appropriateness of the nonlinear term inside the integral is discussed. Among other issues, in [12] the authors did not agree with the fact that cells are attracted by moderately populated areas. Accordingly, to soften the potential strong aggregation they proposed instead a modification of the APS model, where they kept  $g(u) = u$  but multiplied the nonlocal term with a coefficient that ensures saturation. Inspired by this proposal, in the next section we derive a discrete model that in the macroscopic limit yields the model from [12].

**3.3. Motion due to aggregation through nonlocal term with local saturation coefficient** [12]. As before, the dynamics is determined by the result of the gain-loss balance

$$G_{\text{int}}(t, j) - L_{\text{int}}(t, j) = s_{j+1}(t) P_{I_{j+1} \rightarrow I_j}(t) - s_j(t) P_{I_j \rightarrow I_{j-1}} + s_{j-1}(t) P_{I_{j-1} \rightarrow I_j}(t) - s_j(t) P_{I_j \rightarrow I_{j+1}},$$

where now the transition probabilities include a coefficient  $(1 - u_h(y_j, t))$ , such that

$$P_{I_{j+1} \rightarrow I_j}(t) = (1 - u_h(y_{j+1}, t)) \sum_{i=j-r}^j s_i(t) w(y_{j+1} - y_i)$$

$$P_{I_{j-1} \rightarrow I_j}(t) = (1 - u_h(y_{j-1}, t)) \sum_{i=j}^{j+r} s_i(t) w(y_i - y_{j-1}).$$

Notice that in [12] the variable  $u(x, t)$  is regarded to be bounded by one, representing the proportion of cells at position  $x$  at time  $t$ . Therefore, now we will assume that  $0 \leq u_h(y_j, t) \leq 1$ . Again,  $u_h$  could be seen as a discretization of  $u$  by an appropriate numerical scheme.

We argue as in the previous case. By (3.6), the above probabilities are rewritten as

$$P_{I_{j+1} \rightarrow I_j}(t) = (1 - u_h(y_{j+1}, t)) \left[ \mathcal{G}^- u_h(y_{j+1}, t) + O(h^2) \right],$$

and similarly,

$$P_{I_{j-1} \rightarrow I_j}(t) = (1 - u_h(y_{j-1}, t)) \left[ \mathcal{G}^+ u_h(y_{j-1}, t) + O(h^2) \right],$$

with the operators  $\mathcal{G}_h^-, \mathcal{G}_h^+$  specified in (3.7). Then, using (3.6) we can write the terms

$$\text{Left}(j, t) = h^2 \partial_h^+ \left[ u_h(y_j, t) (1 - u_h(y_j, t)) \mathcal{G}^- u_h(y_j, t) \right] + O(h^3),$$

$$\text{Right}(j, t) = h^2 \partial_h^- \left[ u_h(y_j, t) (1 - u_h(y_j, t)) \mathcal{G}^+ u_h(y_j, t) \right] + O(h^3),$$

with the forward and backward differences with respect to  $y$  variable defined in (3.8).

This proves that

$$(3.12) \quad G_{\text{int}}(t, j) - L_{\text{int}}(t, j) = -h^2 \mathcal{T}_{\text{sat}}^h(y_j, t) + O(h^3),$$

where,

$$(3.13) \quad \mathcal{T}_{\text{sat}}^h(y_j, t) := \partial_h^- \left[ u_h(y_j, t) (1 - u_h(y_j, t)) \mathcal{G}_h^+ u_h(y_j, t) \right] - \partial_h^+ \left[ u_h(y_j, t) (1 - u_h(y_j, t)) \mathcal{G}_h^- u_h(y_j, t) \right].$$

Passing again to the limit formally, assuming that  $u_h \rightarrow u$  as  $h \rightarrow 0$ , one arrives at

$$\lim_{h \rightarrow 0} \mathcal{T}_{\text{sat}}^h(y_j, t) = \frac{\partial}{\partial x} \left( u(x, t) (1 - u(x, t)) (\nabla_{NL} u)(x, t) \right),$$

with the nonlocal term  $\nabla_{NL} u$  given in (3.11).

**3.4. Motion due to aggregation/repulsion through nonlocal term with nonlocal saturation coefficient.** One of our main objectives in this paper is to include the effect of repulsion as part of the cells interaction, via a nonlocal coefficient. With this aim in mind, let us consider now a nonlocal saturation coefficient in the transition probabilities for cells positioned at  $I_j$  as follows:

$$(3.14) \quad 1 - \frac{1}{K} \sum_{i=j-r}^{j+r} s_i(t) = 1 - \frac{1}{K} \mathcal{U}_h(y_j, t),$$

being

$$\mathcal{U}_h(y_j, t) = \int_{\bigcup_{i=j-r}^{j+r} I_i} u_h(y, t) dy.$$

Here, the parameter  $K \in (0, 1)$  represents a threshold of nonlocal type for the crowding capacity in the interval  $[x_j - rh, x_j + rh]$  for each  $x_j \in [-L, L]$  (recall that  $r = r(h)$ , such that  $r(h) = [R/h]$ ). We could also ponder the influence of neighboring cells through a non-constant weight  $\hat{w} = \hat{w}(r)$ , namely changing (3.14) by

$$1 - \frac{1}{K} \sum_{i=j-r}^{j+r} s_i(t) \hat{w}(|y_j - y_i|).$$

To make the presentation of the model simpler, we take  $\hat{w} \equiv 1$ . Indeed, as Figures 14 and 15 show, the choice  $\hat{w}(r) = (R - r)/R$  allows more aggregation for the same value of that crowding capacity. Indeed

high accumulations arise for  $\widehat{w}$  linear decreasing, in contrast to Figures 12 and 13 where  $\widehat{w}$  is constant equal to 1.

The nonlocal coefficient (3.14) has the following effect on cell motion: a cell positioned at certain  $I_j$  moves according to aggregation influences whenever the number of cells around its position does not exceed the crowding capacity  $K$ . Above this threshold, the cell begins to move towards less populated areas as a result of repulsion.

As before, cells arriving to  $I_j$  and leaving from  $I_j$  are given by the gain-loss balance:

$$G_{\text{int}}(t, j) - L_{\text{int}}(t, j) = s_{j+1}(t)P_{I_{j+1} \rightarrow I_j}(t) - s_j(t)P_{I_j(t) \rightarrow I_{j-1}} + s_{j-1}(t)P_{I_{j-1} \rightarrow I_j}(t) - s_j(t)P_{I_j(t) \rightarrow I_{j+1}}$$

where the transition probabilities are driven now by two effects. Cells moving from  $I_{j+1}$  towards  $I_j$  (resp. from  $I_{j-1}$  towards  $I_j$ ) engage in two processes: aggregation produced by cells at left hand side inside the sensing radius (resp. at right hand side) and saturation produced by the existing cells at right hand side (resp. at left hand side). To be more precise, denoting as  $(g)_- = \min\{g, 0\}$  and  $(g)_+ = \max\{g, 0\}$  (hence  $g = (g)_+ + (g)_-$ ), we will split the nonlocal saturation coefficient (3.14) into its positive and negative parts representing the conditional transition probabilities due to attraction or repulsion effects, respectively. Accordingly, we define

$$\begin{aligned} P_{I_{j+1} \rightarrow I_j}(t) &= - \left(1 - \frac{1}{K} \mathcal{U}_h(y_{j+1}, t)\right)_- \sum_{i=j+2}^{j+2+r} s_i(t)w(y_i - y_{j+1}) \quad (\text{repulsion term}) \\ &\quad + \left(1 - \frac{1}{K} \mathcal{U}_h(y_{j+1}, t)\right)_+ \sum_{i=j-r}^j s_i(t)w(y_{j+1} - y_i) \quad (\text{aggregation term}) \\ &=: P_{I_{j+1} \rightarrow I_j}(t)_{(1)} + P_{I_{j+1} \rightarrow I_j}(t)_{(2)}, \\ P_{I_{j-1} \rightarrow I_j}(t) &= - \left(1 - \frac{1}{K} \mathcal{U}_h(y_{j-1}, t)\right)_- \sum_{i=j-2-r}^{j-2} s_i(t)w(y_{j-1} - y_i) \quad (\text{repulsion term}) \\ &\quad + \left(1 - \frac{1}{K} \mathcal{U}_h(y_{j-1}, t)\right)_+ \sum_{i=j}^{j+r} s_i(t)w(y_i - y_{j-1}) \quad (\text{aggregation term}) \\ &=: P_{I_{j-1} \rightarrow I_j}(t)_{(1)} + P_{I_{j-1} \rightarrow I_j}(t)_{(2)}. \end{aligned}$$

Now we proceed rewriting these probabilities in terms of the function  $u_h$  in (3.2). For example, let us consider terms  $P_{I_{j+1} \rightarrow I_j}(t)_{(1)}$  and  $P_{I_j \rightarrow I_{j-1}}(t)_{(1)}$ , corresponding to gain and loss by repulsion effects. Indeed, we can express

$$\begin{aligned} &s_{j+1}(t)P_{I_{j+1} \rightarrow I_j}(t)_{(1)} \\ &= -h u_h(y_{j+1}, t) \left(1 - \frac{1}{K} \mathcal{U}_h(y_{j+1}, t)\right)_- \left[\mathcal{G}_h^+ u_h(y_{j+1}, t) + O(h^2)\right] \\ &= -h \left[u_h(y_{j+1}, t) \left(1 - \frac{1}{K} \mathcal{U}_h(y_{j+1}, t)\right)_- \mathcal{G}_h^+ u_h(y_{j+1}, t)\right] + O(h^3), \end{aligned}$$

with  $\mathcal{G}_h^+$  specified in (3.7). Similarly, one has that

$$s_j(t)P_{I_j \rightarrow I_{j-1}}(t)_{(1)} = -h \left[u_h(y_j, t) \left(1 - \frac{1}{K} \mathcal{U}_h(y_j, t)\right)_- \mathcal{G}_h^+ u_h(y_j, t)\right] + O(h^3).$$

In conclusion,

$$\begin{aligned} \text{Left}_{(1)}(j, t) &:= s_{j+1}(t)P_{I_{j+1} \rightarrow I_j}(t)_{(1)} - s_j(t)P_{I_j \rightarrow I_{j-1}}(t)_{(1)} \\ &= -h^2 \left[ \frac{u_h(y_{j+1}, t)(1 - \frac{1}{K}\mathcal{U}_h(y_{j+1}, t)) - \mathcal{G}_h^+ u_h(y_{j+1}, t) - u_h(y_j, t)(1 - \frac{1}{K}\mathcal{U}_h(y_j, t)) - \mathcal{G}_h^+ u(y_j, t)}{h} \right] + O(h^3) \\ &= -h^2 \partial_h^+ \left[ u_h(y_j, t) \left( 1 - \frac{1}{K}\mathcal{U}_h(y_j, t) \right) \mathcal{G}_h^+(y_j, t) \right] + O(h^3), \end{aligned}$$

where we are using the notation in (3.8) for the forward derivative.

Similar arguments for the rest of the terms yield

$$(3.15) \quad G_{\text{int}}(t, j) - L_{\text{int}}(t, j) \sim -h^2 \mathcal{T}_{NL\text{sat}}^h(y_j, t) + O(h^3),$$

where

$$\mathcal{T}_{NL\text{sat}}^h(y_j, t) := \partial_h^- \left[ u_h(y_j, t) \left( 1 - \frac{1}{K}\mathcal{U}_h(y_j, t) \right) \mathcal{G}_h^+ u_h(y_j, t) \right] - \partial_h^+ \left[ u_h(y_j, t) \left( 1 - \frac{1}{K}\mathcal{U}_h(y_j, t) \right) \mathcal{G}_h^- u_h(y_j, t) \right].$$

Passing to the limit (formally), we get

$$\lim_{h \rightarrow 0} \mathcal{T}_{NL\text{sat}}^h(y_j, t) = \frac{\partial}{\partial x} \left( u(x, t) \left( 1 - \frac{1}{K} \int_{x-R}^{x+R} u(y, t) dy \right) \nabla_{NL} u(x, t) \right),$$

where  $\nabla_{NL} u$  is specified in (3.11).

**3.4.1. Boundary effects.** For simplicity, in the descriptions of gain and loss terms given in Sections 3.2, 3.3 and 3.4, we have not taken into account the effects of the boundary, so that our derivations are only valid for  $x \in (-L + R, L - R)$ . We are going to consider isolating boundary conditions, which means that particles can neither enter nor leave the domain. This fact has an influence only for the closest intervals to the boundary. In particular, if capacity is large, cells at the boundary are more likely to be pushed towards the interior by the attraction of other cells, while outside there are not cells, see figures in §5.2 and §5.3. Under strong repulsion the situation is completely different: cells could be pushed towards the boundary, where they then form high accumulation peaks due to its impenetrability, as examples show in §5.4 and §5.5.

**3.5. Dynamics driven by the interplay between diffusion and nonlocal drift.** In this Section we study the combined effect of diffusion with aggregation/repulsion effects and derive the corresponding PDEs. With this aim in mind, let us first specify the gain and loss terms due to diffusion. Following the standard approach that the cells diffuse randomly and, as before, the jump of a cell is of length  $h$ , the proportion of cells arriving to  $I_j$  due to diffusion comes from adjacent intervals, with respective probabilities  $P_{I_{j+1} \rightarrow I_j} = p/2 = P_{I_{j-1} \rightarrow I_j}$  and probability  $1 - p$  of remaining at  $I_j$ . Namely,

$$G_{\text{diff}}(t, j) = s_{j+1}(t)P_{I_{j+1} \rightarrow I_j} + s_{j-1}P_{I_{j-1} \rightarrow I_j} = \frac{p}{2}s_{j+1}(t) + \frac{p}{2}s_{j-1}(t).$$

On the other hand, also by diffusion the cells in the interval  $I_j$  will leave it to travel to either  $I_{j-1}$  or  $I_{j+1}$  with respective probabilities  $P_{I_j \rightarrow I_{j-1}} = p/2 = P_{I_j \rightarrow I_{j+1}}$ . Thus, the proportion of cells leaving  $I_j$  is

$$L_{\text{diff}}(t, j) = s_j(t)(P_{I_j \rightarrow I_{j-1}} + P_{I_j \rightarrow I_{j+1}}) = p s_j(t).$$

Consequently,

$$\begin{aligned}
(3.16) \quad G_{\text{diff}}(t, j) - L_{\text{diff}}(t, j) &= \frac{p}{2}s_{j+1}(t) + \frac{p}{2}s_{j-1}(t) - ps_j(t) \\
&= h\frac{p}{2}\left[(u_h(y_{j+1}, t) - u_h(y_j, t)) + (u_h(y_{j-1}, t) - u_h(y_j, t))\right] \\
&= h^3\frac{p}{2}\left[\Delta_h u_h(y_j)\right],
\end{aligned}$$

where

$$\Delta_h v(x) = \frac{v(x+h) - 2v(x) + v(x-h)}{h^2}$$

is the discrete Laplacian. Then (3.16) can be rewritten as

$$(3.17) \quad G_{\text{diff}}(t, j) - L_{\text{diff}}(t, j) = h^3 \mathcal{T}_{\text{diff}}^h(y_j, t),$$

with

$$\lim_{h \rightarrow 0} \mathcal{T}_{\text{diff}}^h(y_j, t) = \frac{p}{2} \Delta u(x, t).$$

Then, combining (3.1) and (3.17) with the different interaction terms, we deduce the general relation

$$(3.18) \quad h \left[ \frac{u_h(y_j, t + \Delta t) - u_h(y_j, t)}{\Delta t} \right] = Q_{\text{diff}}^h h^3 \mathcal{T}_{\text{diff}}^h(y_j, t) - Q_{\text{int}}^h h^2 (\mathcal{T}^h(y_j, t) + O(h)),$$

where  $\mathcal{T}^h$  is defined either as (3.9), (3.12) or 3.15.

In order to preserve all of the effects in the limit PDEs, the following hypotheses on the frequencies must be imposed:

$$(3.19) \quad \lim_{h \rightarrow 0} h^2 Q_{\text{diff}}^h = \alpha_{\text{diff}},$$

and

$$(3.20) \quad \lim_{h \rightarrow 0} h Q_{\text{int}}^h = \alpha_{\text{int}}.$$

At this stage, it arises the importance of the correct choice of the frequencies  $Q_{\text{diff}}^h$  and  $Q_{\text{int}}^h$ , with respect to  $h$ . See [1], where  $h$  dependent coefficients are taken.

After appropriate time scaling in (3.18), passing formally to the limit as  $\Delta t, h \rightarrow 0$ , we arrive to the general PDE given in (2.1), for each  $x \in (-L, L)$  and  $t > 0$ . Namely,

$$(3.21) \quad u_t(x, t) = u_{xx}(x, t) - \gamma \partial_x \left( u(x, t) K(u)(x, t) \right),$$

where  $\gamma = 2\alpha_{\text{int}}/(p\alpha_{\text{diff}})$  is a positive parameter related to frequencies of interactions and diffusion. The nonlocal drift term  $K(u)$  is given by

3.5.1 Super aggregation APS model [2]:

$$K(u) = \nabla_{NL} u.$$

3.5.2 Local saturation model [12]:

$$K(u) = (1 - u) \nabla_{NL} u.$$

3.5.3 Nonlocal saturation model:

$$K(u)(x, t) = \left( 1 - \frac{1}{K} \int_{x-R}^{x+R} u(y, t) \mathbb{1}_{\Omega}(y) dy \right) \nabla_{NL} u(x, t),$$

where  $\mathbb{1}_{\Omega}$  the characteristic function in  $\Omega$ .

Including the effect of the bounded domain  $\Omega$ , the nonlocal term  $\nabla_{NL}u$  takes the form

$$(3.22) \quad (\nabla_{NL}u)(x, t) = \int_x^{x+R} u(y, t)w(y-x)\mathbb{1}_\Omega(y)dy - \int_{x-R}^x u(y, t)w(x-y)\mathbb{1}_\Omega(y)dy.$$

Moreover, for all of these models, the no-flux boundary conditions read as

$$(3.23) \quad -u_x(x, t) + \gamma u(x, t)K(u)(x, t) = 0, \quad x = -L, L.$$

#### 4. LAGRANGIAN PERSPECTIVE

While in Section 3 we modelled cell densities distributed among intervals, here we choose a Lagrangian perspective, following the motion of individual cells. This optics is particularly useful when the number of cells in the population is not very large. In this way we expect to extract additional features from cell interactions. Thus each perspective reveals complementary information with respect to the other while, on the other hand, they not only give rise identical PDEs, but also they are closely related at the discrete level, as subsequent simulations will reveal.

Now, agent based models are derived where the unknown variable is the position of the cells at certain time  $t$ . As in Section 3 we start by considering a single population of  $N$  cells randomly distributed in  $\Omega = (-L, L)$ , at initial positions  $x_i(0)$ ,  $i = 1, \dots, N$ . The following system of stochastic differential equations describes how the position  $x_i(t)$  of the  $i$ -th cell evolves over time:

$$(4.1) \quad dx_i(t) = \frac{1}{N} \sum_{j \neq i} \mathcal{F}(x_i(t), x_j(t), S_a(x_i))dt + \sqrt{2} \varepsilon B_t^i, \quad i = 1, \dots, N, t > 0.$$

Here,  $\mathcal{F}(x_i, x_j, S_a(x_i))$  represents the action of particle  $j$  on particle  $i$ , that is, the model evolves with pairwise interactions. In case of the APS aggregative interactions, described in §3.2, cells experiment attractive pairwise forces towards the cells within their sensing area. Indeed,  $\mathcal{F}(x_i, x_j, S_a(x_i)) = F(|x_i - x_j|)$ , with  $|\cdot|$  denoting the Euclidean distance. However, the attraction that cell  $j$  exerts on cell  $i$  could be weakened if the neighbouring area to position  $x_i$  is too crowded, or it could become even repulsive. This fact is taken into account by the term  $S_a(x_i)$ , which for the interactions treated in §3.3 and §3.4 will be an appropriate nonlocal saturation or repulsive coefficient of the individual forces acting on particle  $i$ . Namely, these pairwise forces are of the form

$$(4.2) \quad \mathcal{F}(x_i, x_j, S_a(x_i)) = S_a(x_i)F(|x_i - x_j|).$$

The terms  $(B_t^i)$ ,  $i = 1, \dots, N$ ,  $t \geq 0$  denote independent standard Brownian motions on  $\mathbb{R}$ . To ensure then that the particles remain inside the domain, the trajectories given by (4.1) must be truncated such that  $x_i(t) \in [-L, L]$ , for all  $t \geq 0$ .

Systems as (4.1) are classic in many contexts in physics, biology, economics, sociology, etc., where it is necessary to analyze the motion of a large number of particles described their positions, combining deterministic and stochastic processes. The existing literature in this field is vast and increasing over time due to its great applicability. For a general overview on this topic and specific applications to biological processes, such as population dynamics including logistic growth and repulsion effects, tumoral cell growth, applications to finance and market analysis, we refer to the book [8] and references therein. For further references in stochastic equations with applications in swarming we refer to the Chapter [11], and for those related to fluid mechanics, granular flows, traffic models, or large communications networks [3], and references included in these compilations.

In the so-called hydrodynamic limit (as  $N \rightarrow \infty$ ) the independent Brownian motions produce diffusion, while the average sums of (4.1) lead to the different drift terms corresponding to each of the models, depending on the choice of the saturation coefficient  $S_a$ . The continuous density of cells in the

limit  $N \rightarrow \infty$ , denoted by  $u$ , will be a weak solution to mean field deterministic PDEs of the form

$$u_t(x, t) = \varepsilon^2 u_{xx} - \partial_x \left( u(x, t) K(u)(x, t) \right),$$

where  $K(u)(x, t)$  takes into account the balance of the forces exerted on the particles placed on  $x$ . After rescaling in time, we can rewrite it as equation (2.1).

Our aim now is to recover the PDE (3.21) for the different choices of  $K(u)$ . According to the nature of the interacting forces, the drift term  $K(u)$  can yield always aggregation, or it could consider saturation or even repulsion effects. This fact will be determined in the SDEs system by the saturation coefficient,  $S_a$ .

The rigorous derivation of the limit PDE from a discrete system of  $N$  stochastic differential equations as  $N \rightarrow \infty$  is beyond the scope of this paper. Nevertheless we include a short presentation following the course notes collected in [5]. The empirical measure of the system of cells is given by

$$\mu_t^N = \frac{1}{N} \sum_{i=1}^N \delta_{x_i(t)},$$

where  $\delta_x$  is the Dirac mass on  $x \in \mathbb{R}$ .

Let  $\varphi : [-L, L] \rightarrow \mathbb{R}$  be an observable function and  $x_t = x(t) \in [-L, L]$  a trajectory of a cell. How does  $\varphi(x_t)$  evolve in time according to  $\mu_t^N$ ? Recalling Itô's formula and system (4.1), one has

$$\begin{aligned} \langle \varphi, \delta_{x_i(t)} \rangle - \langle \varphi, \delta_{x_i(0)} \rangle &= \varphi(x_i(t)) - \varphi(x_i(0)) = \sqrt{2\varepsilon} \int_0^t \frac{d\varphi}{dx}(x_i(s)) dB_s^i \\ (4.3) \quad &+ \int_0^t \left[ S_a(x_i(s)) \frac{1}{N} \sum_{j \neq i} F(x_i(s), x_j(s)) \frac{d\varphi}{dx}(x_i(s)) + \varepsilon^2 \frac{d^2\varphi}{dx^2}(x_i(s)) \right] ds. \end{aligned}$$

The nonlocal saturation/repulsion coefficient for particle  $i$  at time  $t$  has the form

$$(4.4) \quad S_a(x_i(t)) = 1 - \frac{\lambda}{2aK} \langle \widehat{w}(|z - x_i|) \mathbb{1}_{|z - x_i(t)| < a}, \mu_t^N \rangle, \quad 0 < a \leq L, \quad 0 < K \leq 1, \quad \text{and } \lambda \in \{0, 1\}.$$

If  $\lambda = 0$  the forces take into account only aggregation effects, while saturation occurs when  $\lambda = 1$ . Saturation strength will vary according to the value  $0 < K \leq 1$ , representing the crowding capacity. The parameter  $0 < a \leq L$  delimits the region around the  $i$ -th cell where such effect is taken into account. Finally, the weight  $\widehat{w} = \widehat{w}(r)$  moderates the influence of the surrounding cells according to the distance from the position  $x_i(t)$ . At this stage, averaging equation (4.3) in  $(x_i)_{i=1}^N$  yields

$$\begin{aligned} \langle \varphi, \mu_t^N \rangle - \langle \varphi, \mu_0^N \rangle &= \int_0^t \frac{1}{N} \sum_{i=1}^N \left[ \left( 1 - \frac{\lambda}{2aK} \langle \widehat{w}(|z - x_i|) \mathbb{1}_{|z - x_i(t)| < a}, \mu_t^N \rangle \right) \frac{1}{N} \sum_{j \neq i} F(x_i(s), x_j(s)) \frac{d\varphi}{dx}(x_i(s)) \right] ds \\ &+ \int_0^t \frac{1}{N} \sum_{i=1}^N \varepsilon^2 \frac{d^2\varphi}{dx^2}(x_i(s)) ds + \sqrt{2\varepsilon} \int_0^t \frac{1}{N} \sum_{i=1}^N \frac{d\varphi}{dx}(x_i(s)) dB_s^i \\ (4.5) \quad &= \int_0^t \int_{-L}^L \left( 1 - \frac{\lambda}{2aK} \int_{-L}^L \widehat{w}(|z - x|) \mathbb{1}_{|z - x| < a} \mu_s^N(z) dz \right) \left( \int_{-L}^L F(x, y) d\mu_s^N(y) dy \right) \frac{d\varphi}{dx}(x) dx ds \\ &+ \int_0^t \int_{-L}^L \varepsilon^2 \frac{d^2\varphi}{dx^2}(x) d\mu_s^N(x) ds + \sqrt{2\varepsilon} \int_0^t \frac{1}{N} \sum_{i=1}^N \frac{d\varphi}{dx}(x_i(s)) dB_s^i. \end{aligned}$$

It is well known that by the law of large numbers it holds that

$$\sqrt{2\varepsilon} \int_0^t \frac{1}{N} \sum_{i=1}^N \frac{d\varphi}{dx_i}(x_i(s)) dB_s^i \rightarrow 0, \quad \text{as } N \rightarrow \infty.$$

Appropriate hypotheses ensure the existence of a measure  $\mu_t$  absolutely continuous with respect to the spatial variable, such that  $\mu_t^N \rightarrow \mu_t$  as  $N \rightarrow \infty$ . We identify formally the limiting PDEs for each of the cases.

#### 4.1. Strong aggregation (APS) model [2].

Let us begin our analysis with the Lagrangian formulation of the APS model, which exhibits strong aggregation, by taking in the coefficient (4.4) of the pairwise forces (4.2) the parameter  $\lambda = 0$  and defining

$$(4.6) \quad F(x_i, x_j) = \gamma w(|x_i - x_j|) \text{sign}(x_j - x_i)$$

where  $w : [0, +\infty) \rightarrow \mathbb{R}_+$  is a nonnegative weight function with  $w(r) > 0$  for  $r \in [0, R)$  and  $w(r) = 0$  for  $r \geq R$ . For instance  $w(r)$  could be linearly decreasing with respect to the distance  $r = |x_i - x_j|$ . Then, in the limit as  $N \rightarrow \infty$

$$\int_{-L}^L \varphi d\mu_t - \int_{-L}^L \varphi d\mu_0 = \int_0^t \left[ \int_{-L}^L \int_{-L}^L \gamma w(|x - y|) \text{sign}(y - x) d\mu_s(y) \nabla_x \varphi d\mu_s(x) + \varepsilon^2 \Delta \varphi(x) d\mu_s(x) \right] ds,$$

which is the weak form of equation (3.21) with drift term according to model §3.5.1 assuming that  $\mu_t(A) = \int_A u(x, t) dx$ .

Starting from random distributed positions, at first stages, when the cells are still all spread, it is improbable that attraction plays a role far from the boundary. However, when the moving cell has a position  $x_i(t)$  close to the boundary, it experiments an attraction towards the interior where the rest of cells are.

On the other hand, as the density of cells is no longer equally distributed, if these attraction forces are dominant with respect to diffusion, then it might yield to very contractive and highly oscillate dynamics. In the spirit of avoiding it, we will take the value of  $\lambda = 1$  in the saturation coefficient (4.4) and deduce aggregation/saturation models.

**4.2. Nonlocal saturation coefficient.** We propose to consider a nonlocal saturation coefficient (4.4) with  $\lambda = 1$  and choosing  $a = R$  the sensing radius and the forces (4.6). Namely,

$$\mathcal{F}(x_i, x_j, S_R(x_i)) = \left( 1 - \frac{1}{2RK} \langle \widehat{w}(|z - x_i|) \mathbb{1}_{|z - x_i(t)| < R}, \mu_t^N \rangle \right) F(x_i, x_j),$$

for some value of the crowding capacity  $0 < K \leq 1$  and some weight  $\widehat{w} = \widehat{w}(r)$ , linear decreasing with the distance or a positive constant. As numerical simulations will show, choosing  $\widehat{w}$  linearly decreasing is related to take higher crowding capacity  $K$ , permitting more aggregation, as it can be appreciated in Figures 14 and 15. Hence, in the sequel  $\widehat{w} = 1$ . Taking  $N \rightarrow \infty$  in (4.5) yields the PDE (3.21) with drift term corresponding to §3.5.3.

#### 4.3. Local saturation coefficient [12].

Recall that trajectories follow (4.5) according to the nonlocal saturation coefficient (4.4) with  $\lambda = 1$  and pairwise interactions  $F(x_i, x_j)$  specified by (4.6). In the limit  $N \rightarrow \infty$  we wish to obtain the PDE given in (3.21), corresponding to model §3.5.2, thus the nonlocal coefficient (4.4) must converge to the local term  $(1 - u(x, t))$ . For this purpose, we take  $K = 1$  and  $a = a(N)$  such that  $a(N) \rightarrow 0$  as  $N \rightarrow \infty$ . With this choice

$$S_a(x_i(t)) = 1 - \frac{1}{2a} \langle \mathbb{1}_{|z - x_i(t)| < a}, \mu_t^N \rangle = 1 - \frac{1}{2a} \int_{x_i(t) - a}^{x_i(t) + a} d\mu_t^N(z),$$

hence the coefficient  $S_a(x_i(t))$  approaches to the local PDE coefficient  $1 - u$  as  $N \rightarrow \infty$ .

## 5. NUMERICAL SIMULATIONS

We conclude this work by performing some numerical simulations to illustrate how the interaction effects of the different models under consideration act on the diffusive random movements of the cells. We compare the corresponding asymptotic behaviour obtained for each case, when varying the parameters involved. These numerical experiments will also reveal the coherence between both perspectives, Eulerian and Lagrangian, when approaching the corresponding mean field PDEs of each model.

**5.1. Numerical methods.** Notice that the general equation (3.18) could be thought as an explicit Euler time scheme, and centred spatial finite difference approximation of the diffusion and interaction terms, of the resulting PDE. However, such a scheme does not generally give rise to an appropriate numerical method. Indeed, in the case of interaction dominance, strong aggregation and repulsion could eventually destabilize the numerical results.

Willing to avoid this issue, we propose a semi-implicit linear scheme in time combined with an upwind finite volume scheme (of Godunov type) in space, a well known technique widely used when simulating propagating phenomena, see for instance [28]. Roughly speaking, upwind schemes attempt to discretize the equation by using finite differences biased in the direction determined by the sign of the characteristic speed. This technique results a very robust and efficient numerical approach. The interaction term,  $\nabla \cdot (uK(u))$  for different choices of  $K(u)$  in §3.5.1, §3.5.2, §3.5.3, is linearized by approximating the nonlocal term  $K(u)$  explicitly. This way it is possible to keep the sparse structure of the approximating matrices.

Regarding the Lagrangian perspective, recall that the motion of any cell  $i$  adopts the following structure

$$dx_i(t) = \mathcal{F}(\vec{x}(t), S_a(x_i(t)))dt + \varepsilon^2 dB_i(t).$$

The independent Brownian motions are driven by a normal distribution for all  $i = 1, \dots, N$ , precisely  $B_i(t) = \mathcal{N}(0, 0.1)$ , and the diffusion coefficient is considered to be constant  $\varepsilon^2 = 0.4$ .

We approximate the deterministic part of the trajectories using Euler explicit scheme and sample the normal distribution to reproduce the Brownian motion. Namely,

$$(5.1) \quad x_i(t + \Delta t) = x_i(t) + \Delta t[\mathcal{F}(\vec{x}(t), S_a(x_i(t))) + \varepsilon^2 \mathcal{N}(0, 0.1)].$$

The choice of saturation coefficient  $S_a$ , specified in (4.4), will vary in order to depict the three different models studied in the previous section.

In all of the simulations we can appreciate the consistency between both perspectives, Eulerian and Lagrangian. From the set of trajectories of the SDEs system, we compute the drift terms of the different models, §3.5.1, §3.5.2, §3.5.3, and their corresponding saturation coefficients in the cases §3.5.2, §3.5.3, according to a fix mesh in the spatial variable. When obtaining the drifts §3.5.1 and §3.5.3 from the SDEs system, we take a mesh of size  $\hat{h} > 0$  independent of the number of cells. However, to approximate the local coefficient in §3.5.2 by the nonlocal coefficient (4.4), is more delicate than in the other two cases. In this particular approach we need  $\hat{h}$  to depend on the number of cells  $N$ . Precisely, we take  $\hat{h} = 2/\sqrt{N}$ .

**Common parameters:** All of the subsequent simulations are performed in the domain  $\bar{\Omega} = [-1, 1]$ , choosing the sensing radius to be  $R = 0.5$ . The interactions among cells are weighted by (3.3), which in most of the cases will be taken inversely proportional to their distance as  $w(r) = (R - r)/R$  and just in some cases being constant  $w \equiv 1$ , precisely in Figures 8, 9, 22 and 23. On the other hand, in Figures 14 and 15 we investigate the impact of considering a weight  $\hat{w}(r) = (R - r)/R$  in the nonlocal

saturation coefficient in §3.5.3 and in the SDEs system §4.2 in contrast to  $\hat{w} \equiv 1$ , as in the rest of the examples related to this model.

In case of Eulerian simulations we use a uniform spatial mesh of size  $h = 2 \cdot 10^{-3}$  and time step  $\Delta t = 10^{-4}$ . The number of time iterations will depend on the example under consideration, needing to be higher as the saturation is stronger. It is also essential to calibrate the frequency of occurrence of both mechanisms, diffusion and interactions. This is recorded in the parameter  $\gamma$  accounting for the relative frequency between them. Indeed, recall that  $\gamma = 2\alpha_{\text{int}}/(p\alpha_{\text{diff}})$ , with  $\alpha_{\text{int}}$  and  $\alpha_{\text{diff}}$  specified in (3.19) and (3.20), respectively and  $p \in (0, 1)$  the probability of moving randomly at one time step  $\Delta t$ . We take the value  $\gamma = 10^3$ .

In the Lagrangian perspective, for cases 4.1 and 4.2 we start with  $N \sim 300$ , use a time step  $\Delta t = 0.01$  and a mesh  $\hat{h} = 0.01$  to depict the drift and saturation coefficients. As we mentioned, model 4.3 is more delicate. We start with  $N \sim 3000$  and reduce the time step  $\Delta t = 0.001$ , which increases the number of iterations. In addition, a mesh of size  $\hat{h} = 2/\sqrt{N}$  is needed to obtain a representation of the drift terms and saturation coefficients as similar as possible to §3.5.2 and histograms resembling the solutions of the PDEs.

In the sequel we include several examples illustrating all of the models for different values of the parameter  $K \in (0, 1]$  regulating the crowding capacity, combined with diverse choices of weights  $w$  and  $\hat{w}$ . We compare the pictures obtained for Eulerian and for Lagrangian perspectives. In all of these examples, the initial configuration of the cells is uniformly distributed, either along the whole domain  $[-L, L]$  or, as in Figures 16, 17, 26, 27 concentrated in some  $[-\delta, \delta]$ . This option corresponds to take as initial datum a perturbation of an appropriated constant, either  $1/(2L)$  or  $1/(2\delta)$  in the Eulerian perspective.

**Numerical simulations description:** We include several examples for the three models treated in this work considering different intensities for repulsion. Precisely, absence of repulsion ( $K = 1$ ), weak repulsion ( $K = 0.6$ ), intermediate repulsion ( $K = 0.4$ ) and strong repulsion ( $K = 0.2$ ).

*Absence of repulsion:* Figures 1 and 2 are devoted to illustrate the APS model, for which high accumulations peaks are formed. In contrast, even for high values of  $K$ , notice that the local saturation model prevents the formation of these strong aggregations. Figures 3 and 5 correspond to  $K = 1$ . As we mentioned, the approach of the local saturation coefficient  $1 - u$  by the discrete saturation coefficients  $S_a$  given in Section §4.3 needs high values of  $N$ . We take  $N = 3.500$  and  $a(N) = 1/\sqrt{N}$ , (hence  $a(N) \rightarrow 0$ , as  $N \rightarrow \infty$ ). The time step is reduced to  $\Delta t = 0.001$ . However, we cannot avoid that the saturation coefficient  $S_a$  of model §4.3 eventually becomes negative, as it is depicted in Figure 5. Nevertheless, the correspondence of both dynamics, Eulerian and Lagrangian is quite coherent, as it can be appreciated in Figures 3 and 4. In the absence of repulsion, the nonlocal saturation model avoids as well the formation of accumulations peaks, but only considering a constant weight  $w \equiv 1$  in the nonlocal term, see Figures 8 and 9. For a linear decreasing weight  $w$  and  $K = 1$  Figures 6 and 9 show strong aggregations.

*Weak repulsion:* As repulsion slightly grows,  $K = 0.6$ , particles tend to spread more distributed along the domain. This dissemination is more evident and uniform in case of the local saturation coefficient model, see Figures 10 and 11. In contrast, considering the nonlocal saturation model in §4.2, cells move more aggregated and towards the interior of the domain, see Figures 12 and 13, and accumulate at

the boundary of the “aggregation tubes”. The non-locality of the saturation coefficient allows higher accumulations on such boundaries. In this range of weak repulsion we have also depicted the case of a constant weight  $\hat{w} \equiv 1$ . This choice of weight in the coefficient reduces the saturation, hence accused peaks are formed, as Figures 14 and 15 reveal. We conclude this subsection by investigating the evolution of a uniformly concentrated initial data in the interval  $[-0.3, 0.3]$  when  $K = 0.6$ . The dynamics reduces approximately to the interval  $[-0.2, 0.2]$ , with accumulations at the boundaries. It can be observed in Figures 16 and 17.

*Intermediate repulsion:* Increasing repulsion, ( $K = 0.4$ ), the local saturation model §4.3 spreads the cells along the whole domain. In contrast to the choice  $K = 0.6$ , if  $K = 0.4$  cells accumulate at the boundaries. This fact can be observed in Figures 18 and 19. Regarding nonlocal saturation model §4.2, the saturation effect acts in a larger set than in the case  $K = 0.6$ . This fact disseminates the cells wider than with less repulsion and, as before, accumulated at the boundaries of the aggregation tubes, see Figures 20 and 21. Choosing  $\hat{w} \equiv 1$  in the nonlocal coefficient introduces repulsion, given that all of the existing cells inside the sensing radius have the same importance. Consequently, cells are pushed towards the boundaries, though there exit some aggregations in the interior, see Figures 22 and 23.

*High repulsion:* In the local saturation model §4.3, reducing the crowding capacity up to  $K = 0.2$  produces no significant change to the case  $K = 0.4$ , hence we do not include the simulations. With respect to nonlocal saturation model §4.2, the cells spread now along the whole domain, Figures 24 and 25, even when starting with concentrated data, Figures 26 and 27.

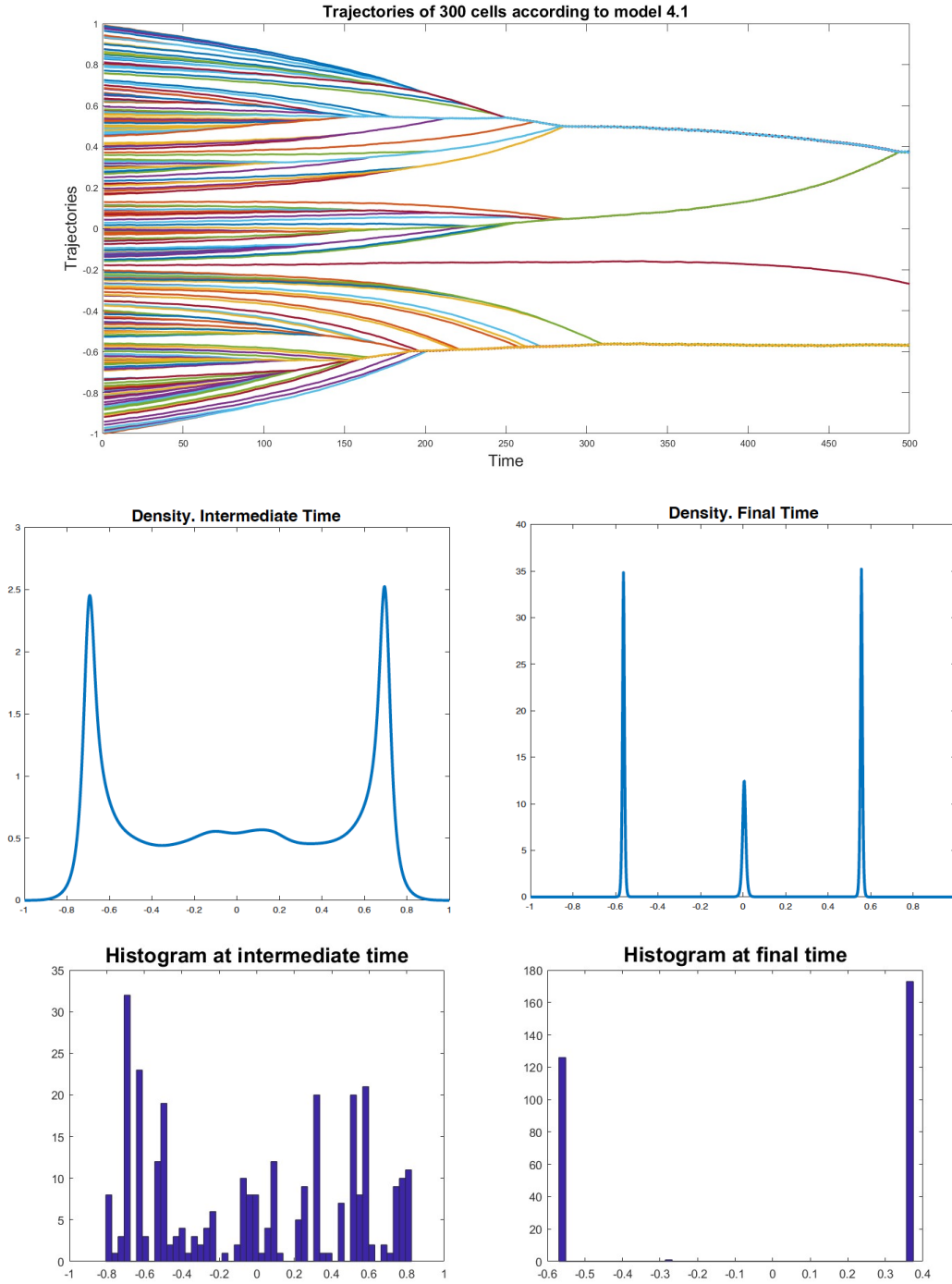
5.2. Absence of repulsion  $K = 1$ .

FIGURE 1. APS model. First row trajectories with  $N = 300$  cells, second row densities of the PDE model (§3.5.1) and third one histograms of SDEs (§4.1). Both at intermediate time on the left and at final time on the right.

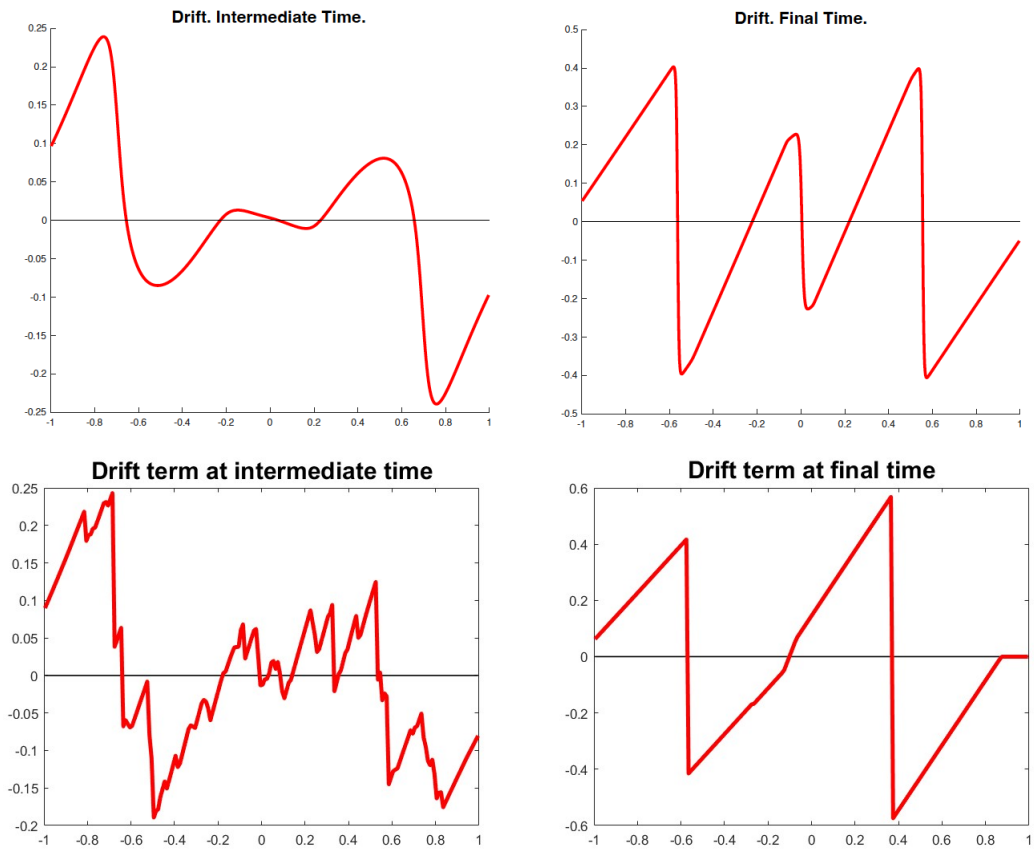


FIGURE 2. Drifts for APS model. First row PDE model (§3.5.1) and second row SDEs (§4.1). Both at intermediate time on the left and at final time on the right.

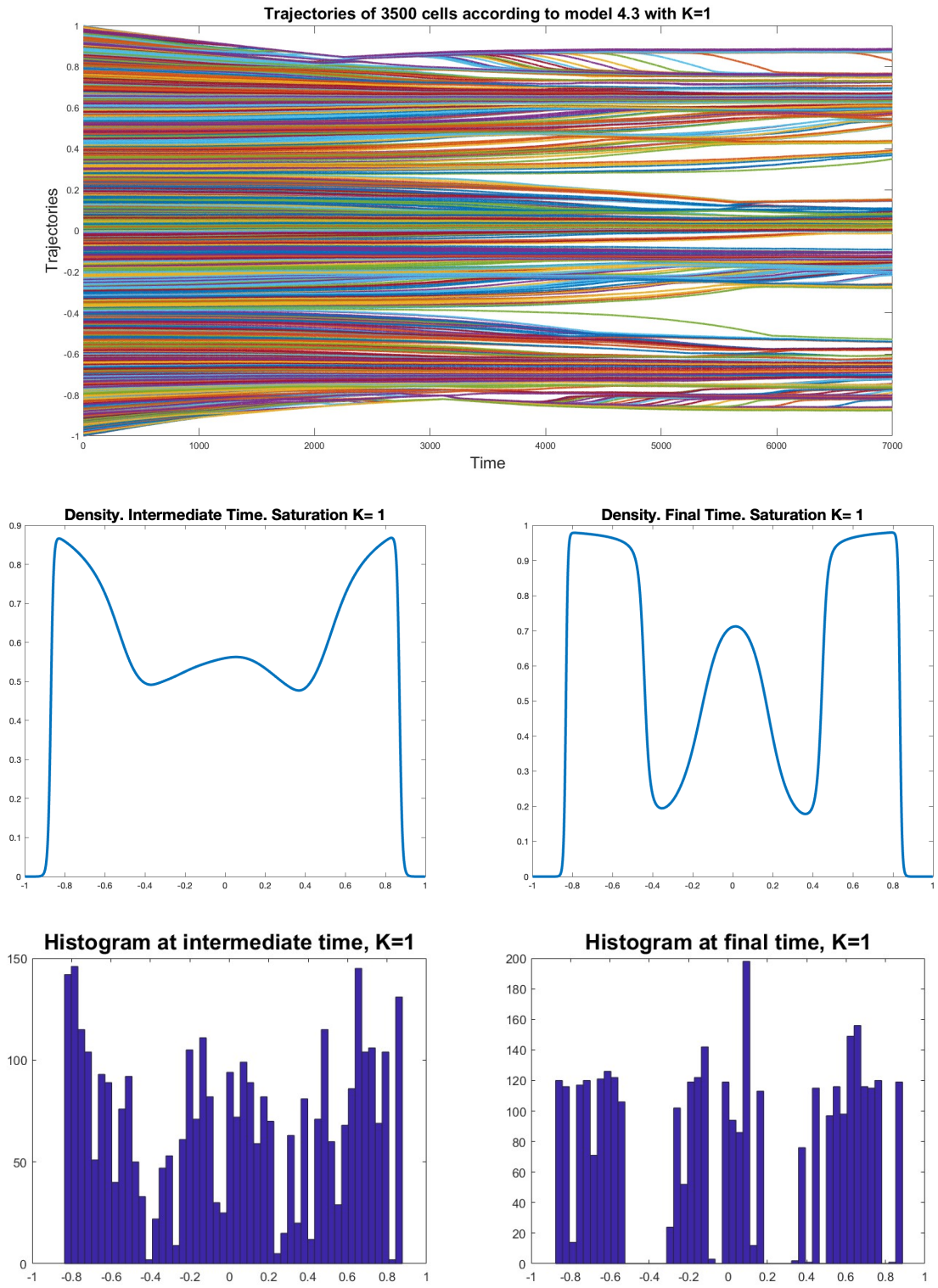


FIGURE 3. Local saturation model,  $K = 1$ . First row trajectories with  $N = 3500$  cells, second row densities of the PDE model (§3.5.2) and third one histograms of SDEs (§4.3). Both at intermediate time on the left and at final time on the right.

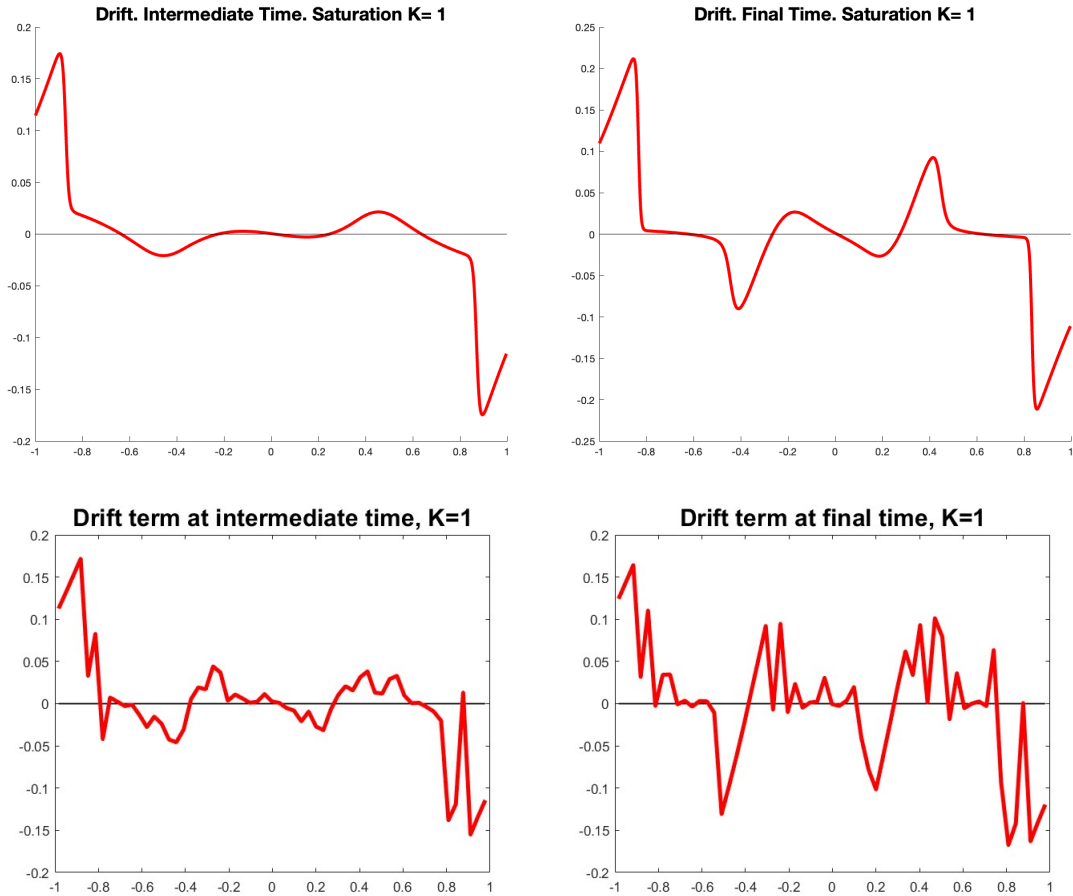


FIGURE 4. Local saturation model,  $K = 1$ . First row trajectories with  $N = 3500$  cells, second row densities of the PDE model (§3.5.2) and third one histograms of SDEs (§4.3). Both at intermediate time on the left and at final time on the right.

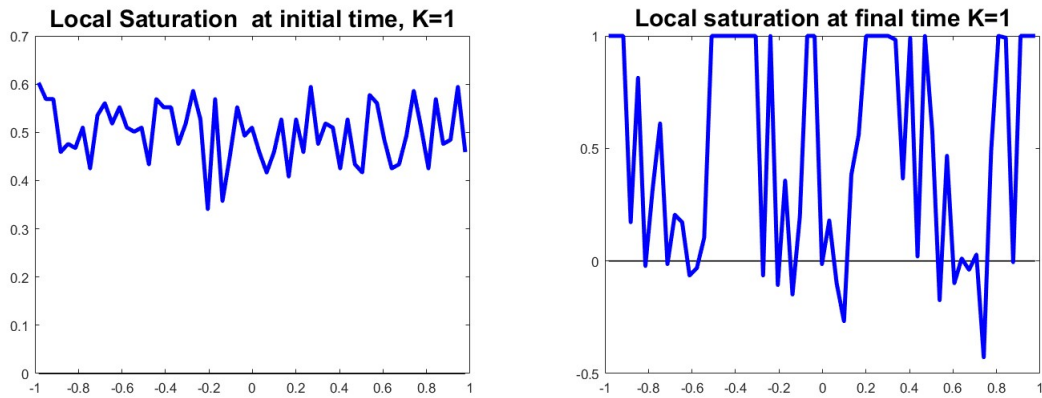


FIGURE 5. Local saturation coefficients for SDEs (§4.3),  $K = 1$ . Initial time on the left and final time on the right.

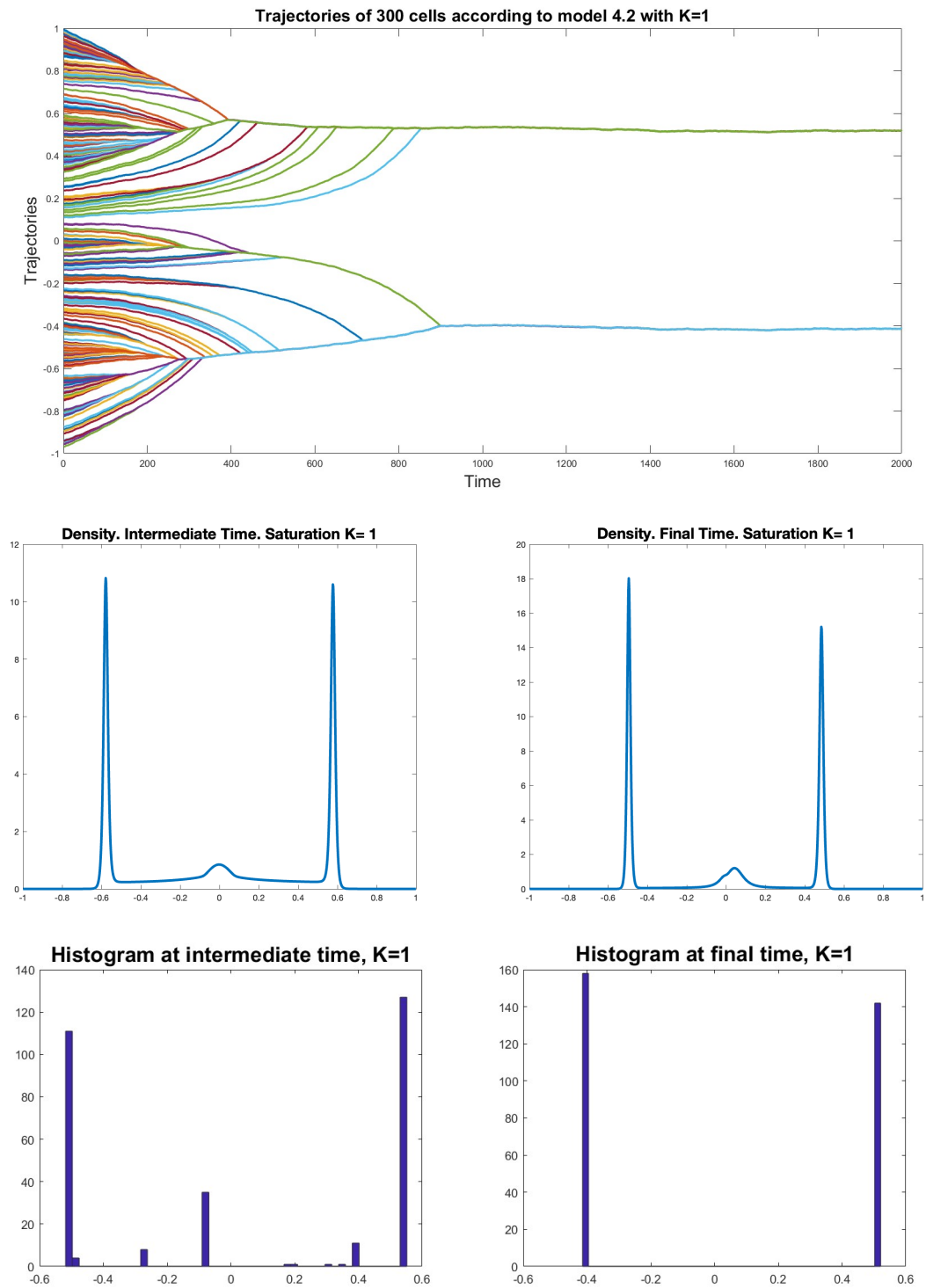


FIGURE 6. Nonlocal saturation model,  $K = 1$ . First row trajectories with  $N = 300$  cells, second row densities of the PDE model (§3.5.3) and third one histograms of SDEs (§4.2). Both at intermediate time on the left and at final time on the right.

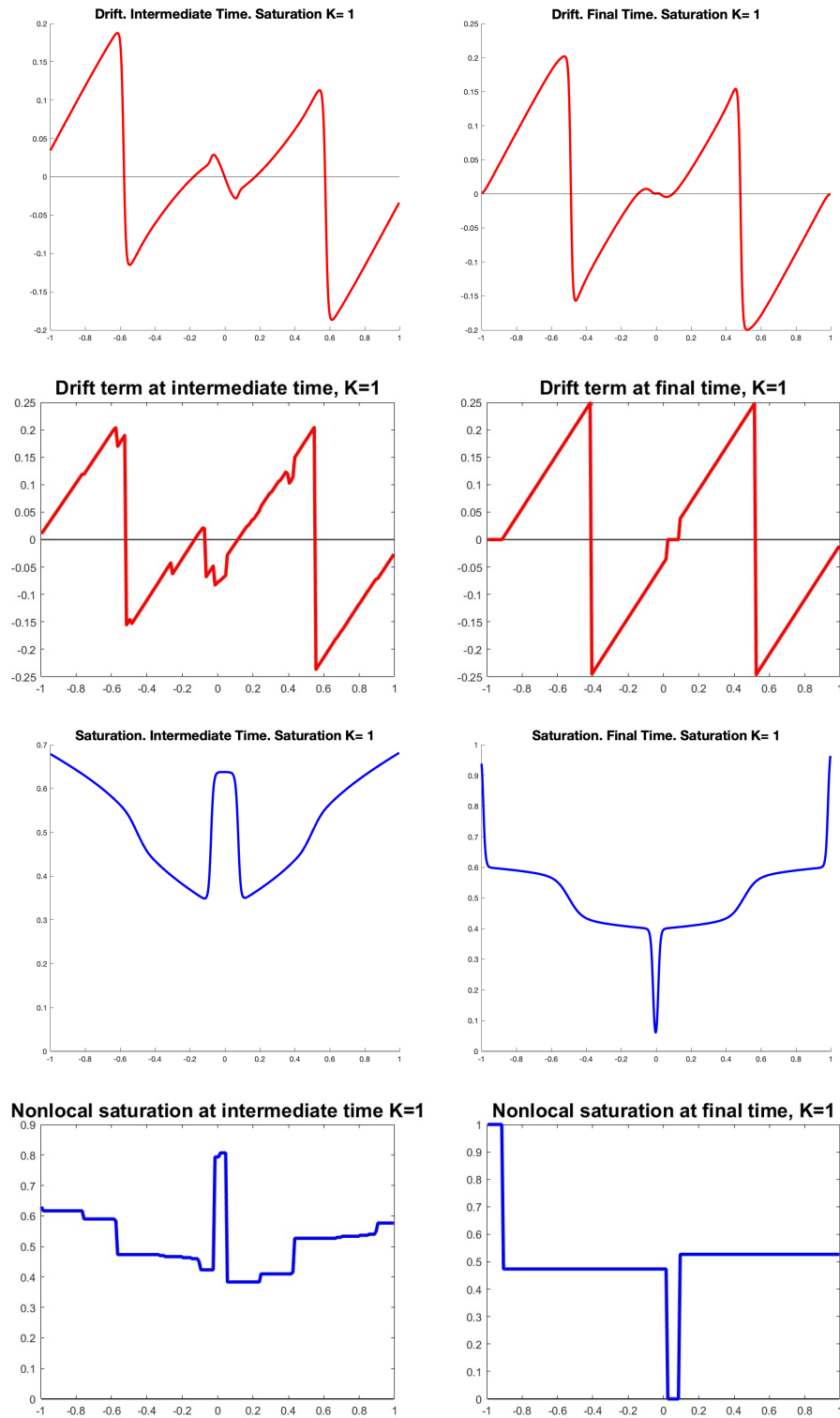


FIGURE 7. Drifts and saturations for nonlocal saturation model,  $K = 1$ . Drifts in first and second rows for PDE model (§3.5.3) and SDEs (§4.2), respectively. Saturations in third and fourth rows for PDE model (§3.5.3) and SDEs (§4.2), respectively. All of them at intermediate time on the left and at final time on the right.

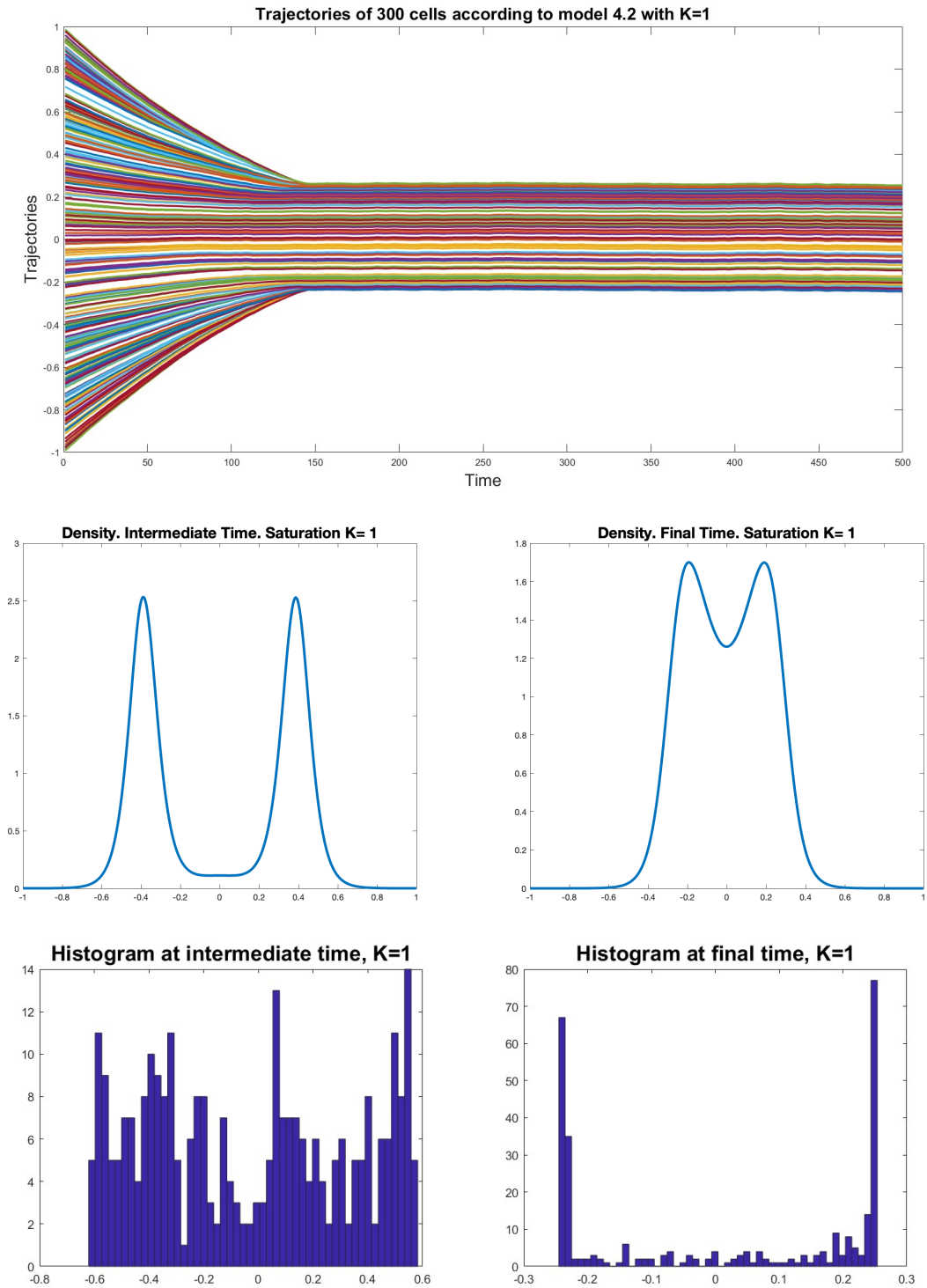


FIGURE 8. Nonlocal saturation model,  $K = 1$  and constant weight. First row trajectories with  $N = 300$  cells, second row densities of the PDE model (§3.5.3) and third one histograms of SDEs (§4.2). Both at intermediate time on the left and at final time on the right.

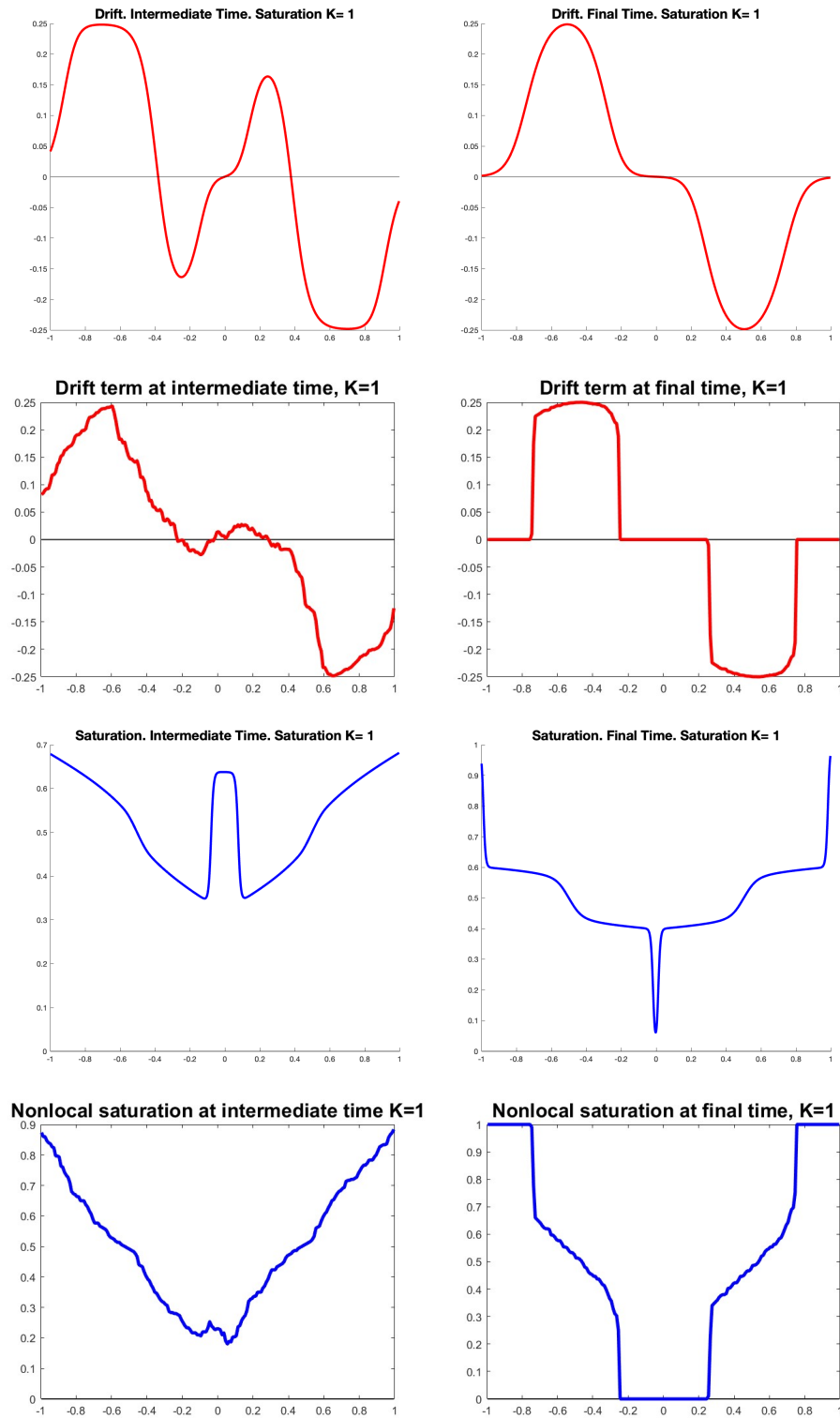


FIGURE 9. Drifts and saturations for nonlocal saturation model,  $K = 1$  and constant weight. Drifts in first and second rows for PDE model (§3.5.3) and SDEs (§4.2), respectively. Saturations in third and fourth rows for PDE model (§3.5.3) and SDEs (§4.2), respectively. All of them at intermediate time on the left and at final time on the right.

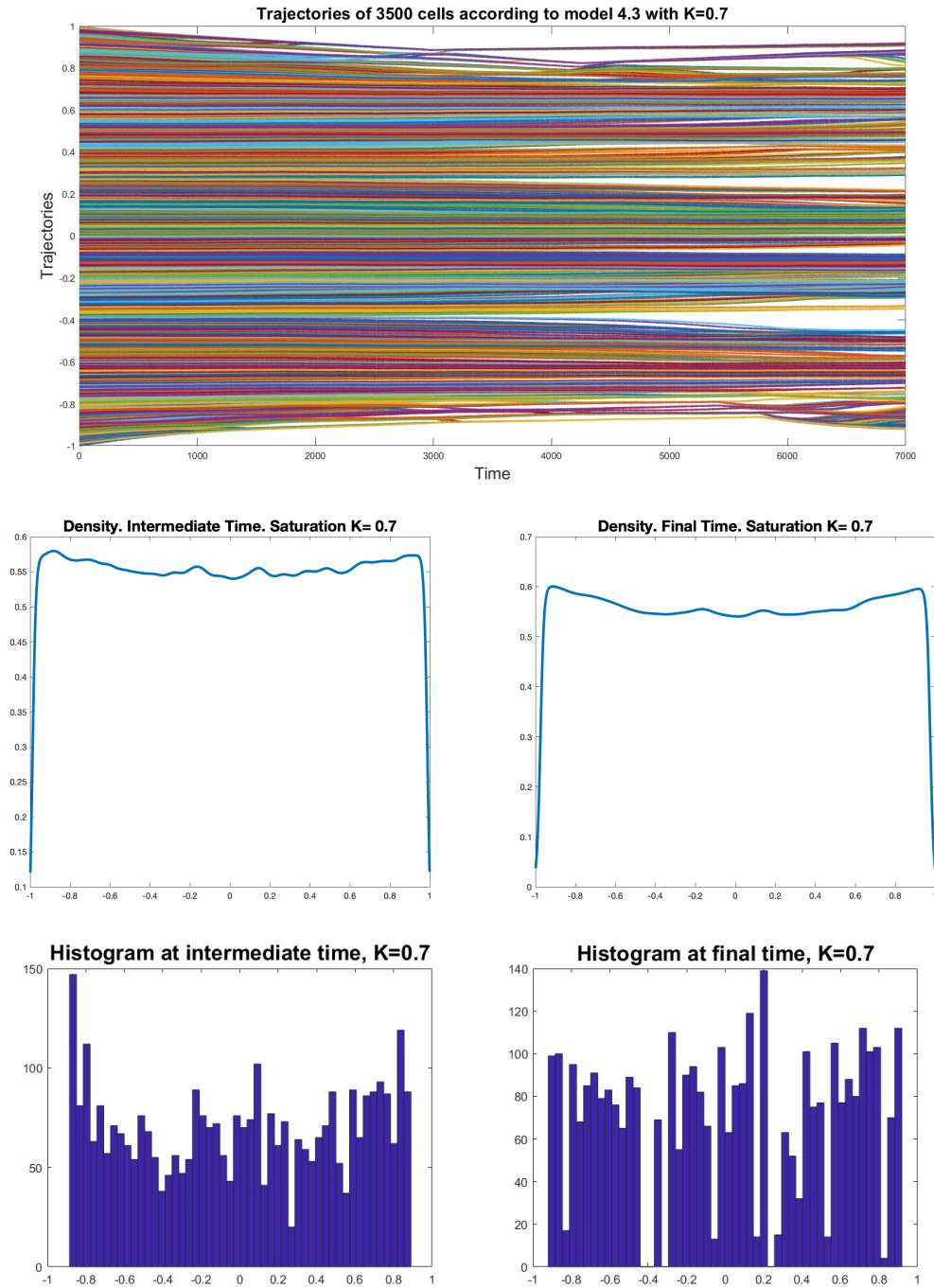
5.3. Weak repulsion  $K \sim 0.6$ .

FIGURE 10. Local saturation model,  $K = 0.7$ . First row trajectories with  $N = 3500$  cells, second row densities of the PDE model (§3.5.2) and third one histograms of SDEs (§4.3). Both at intermediate time on the left and at final time on the right.

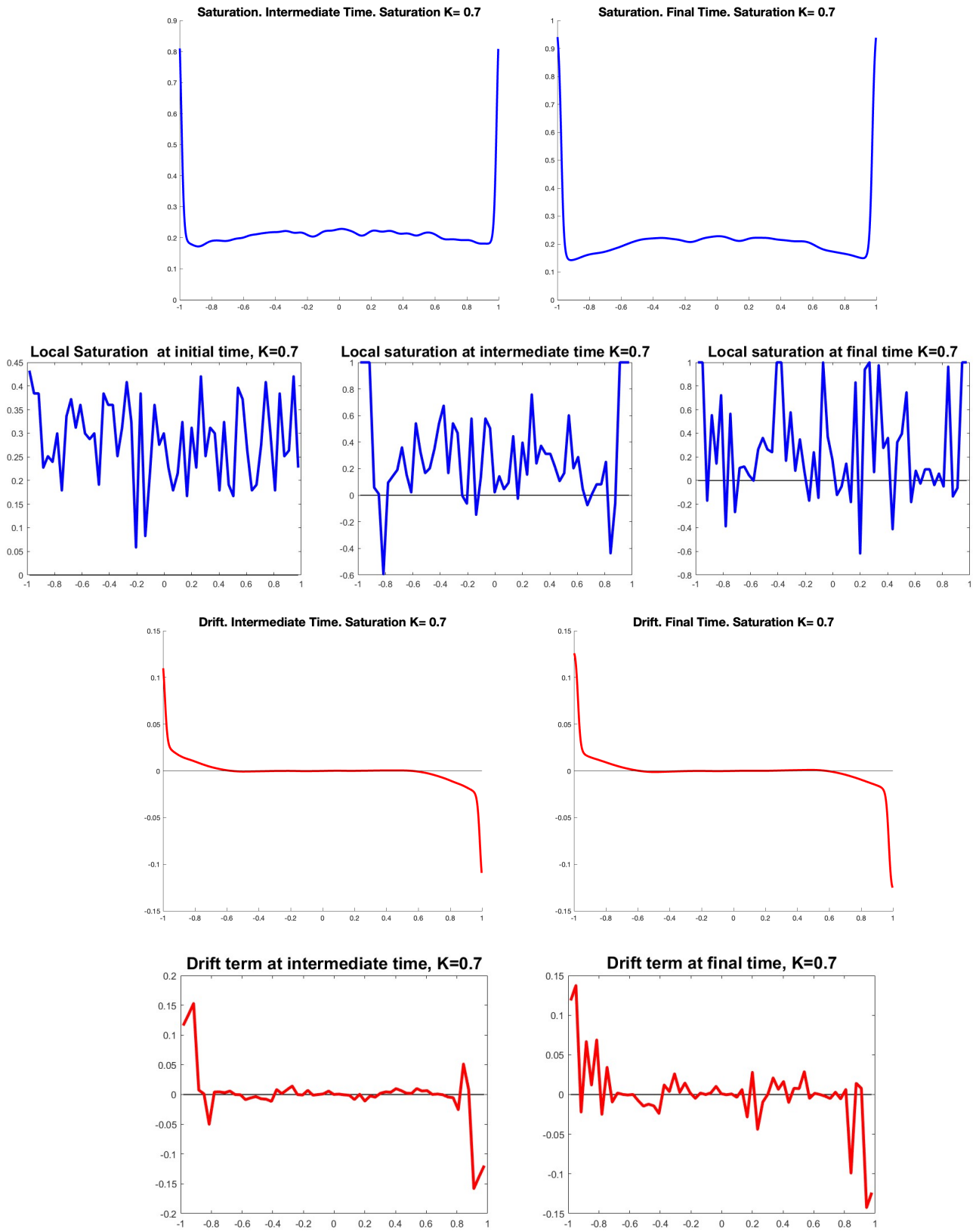


FIGURE 11. Local saturation coefficients and drifts for PDE model (§3.5.3) and SDEs (§4.2), respectively  $K = 0.7$ .

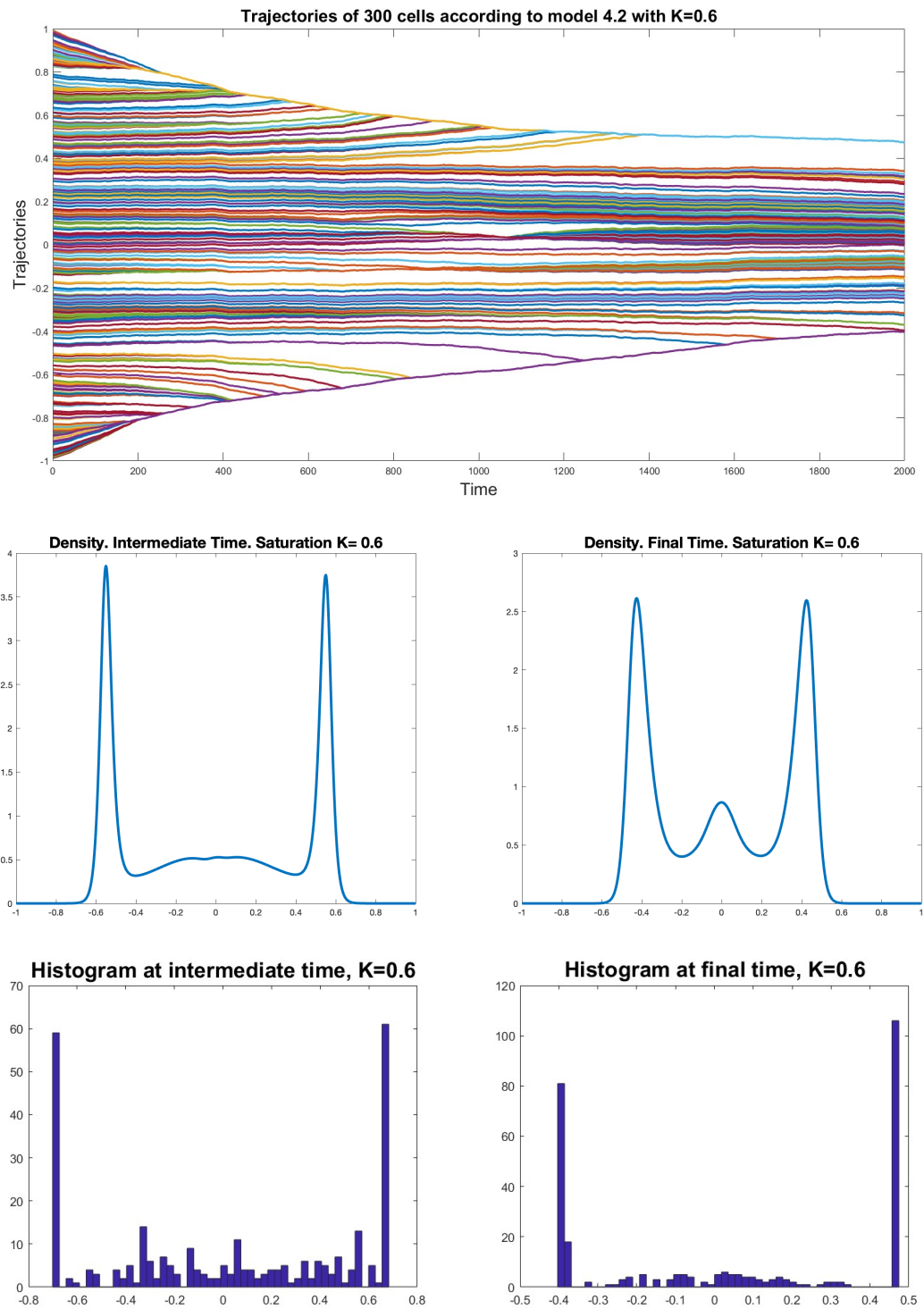


FIGURE 12. Nonlocal saturation model,  $K = 0.6$ . First row trajectories with  $N = 300$  cells, second row densities of the PDE model (§3.5.3) and third one histograms of SDEs (§4.2). Both at intermediate time on the left and at final time on the right.

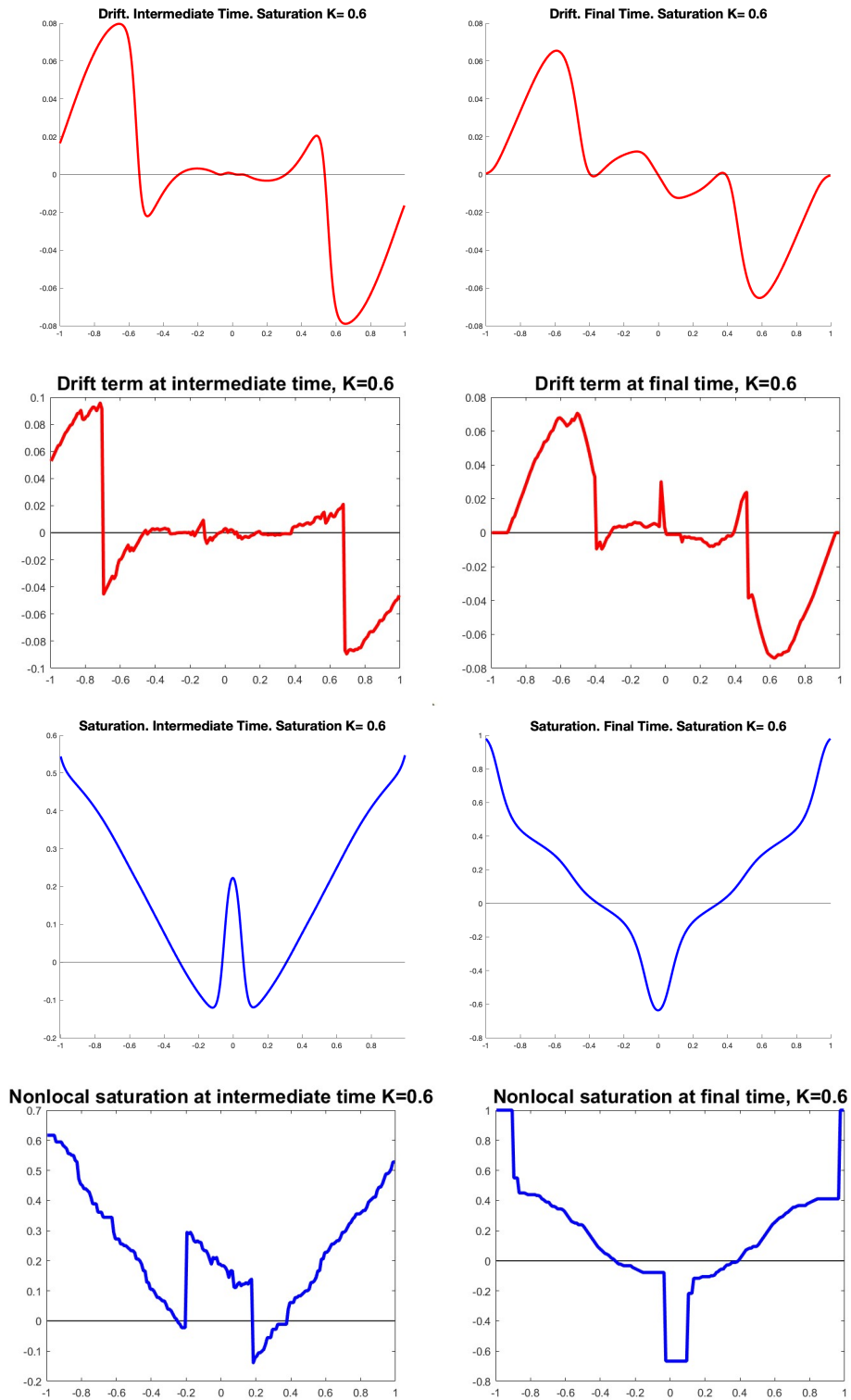


FIGURE 13. Drifts and saturations for nonlocal saturation model,  $K = 0.6$ . Drifts in first and second rows for PDE model (§3.5.3) and SDEs (§4.2), respectively. Saturations in third and fourth rows for PDE model (§3.5.3) and SDEs (§4.2), respectively. All of them at intermediate time on the left and at final time on the right.

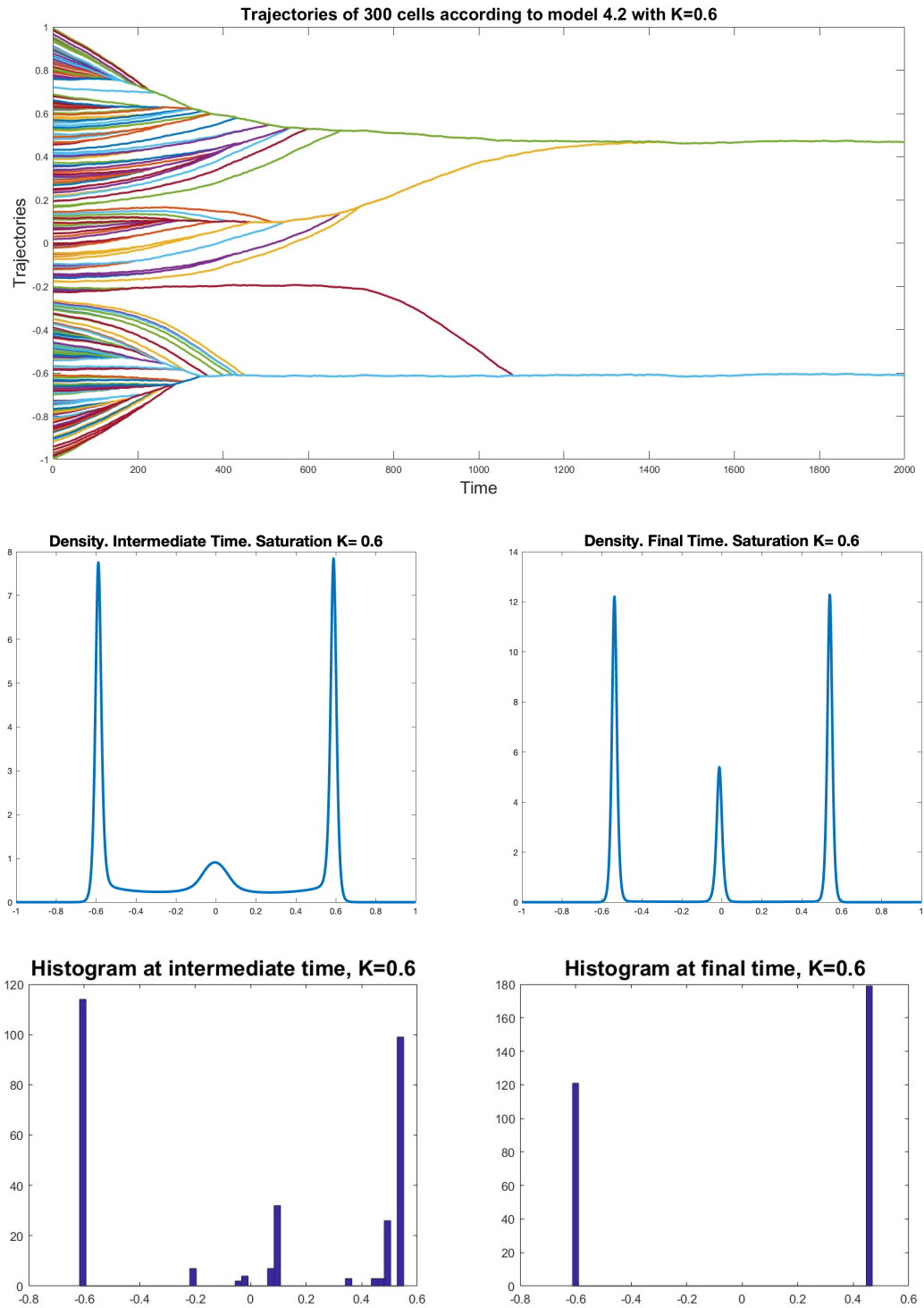


FIGURE 14. Nonlocal saturation model,  $K = 0.6$ , linear weight in saturation. First row trajectories with  $N = 300$  cells, second row densities of the PDE model (§3.5.3) and third one histograms of SDEs (§4.2). Both at intermediate time on the left and at final time on the right.

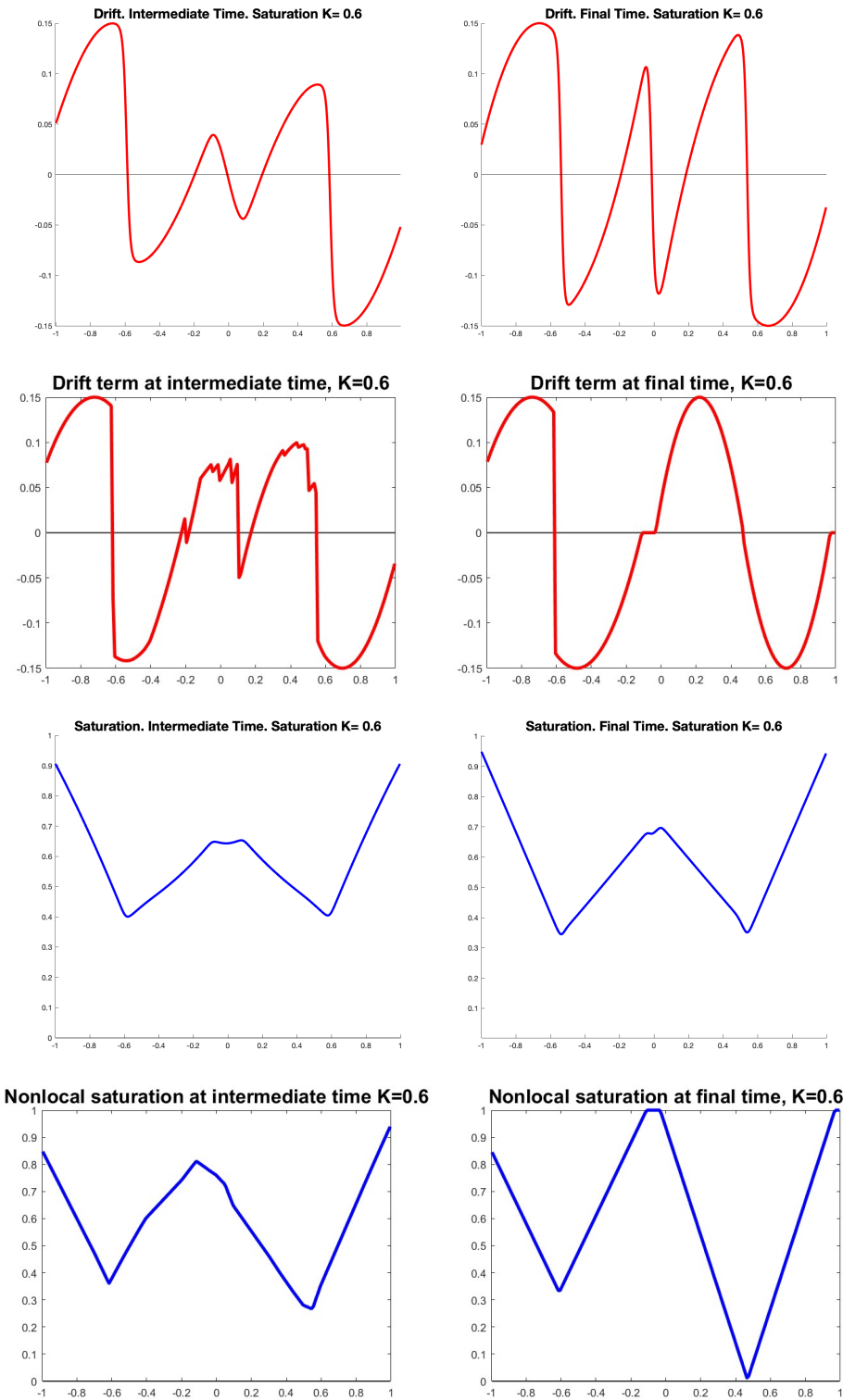


FIGURE 15. Drifts and saturations for nonlocal saturation model,  $K = 0.6$ , linear weight in saturation. Drifts in first and second rows for PDE model (§3.5.3) and SDEs (§4.2), respectively. Saturations in third and fourth rows for PDE model (§3.5.3) and SDEs (§4.2), respectively. All of them at intermediate time on the left and at final time on the right.

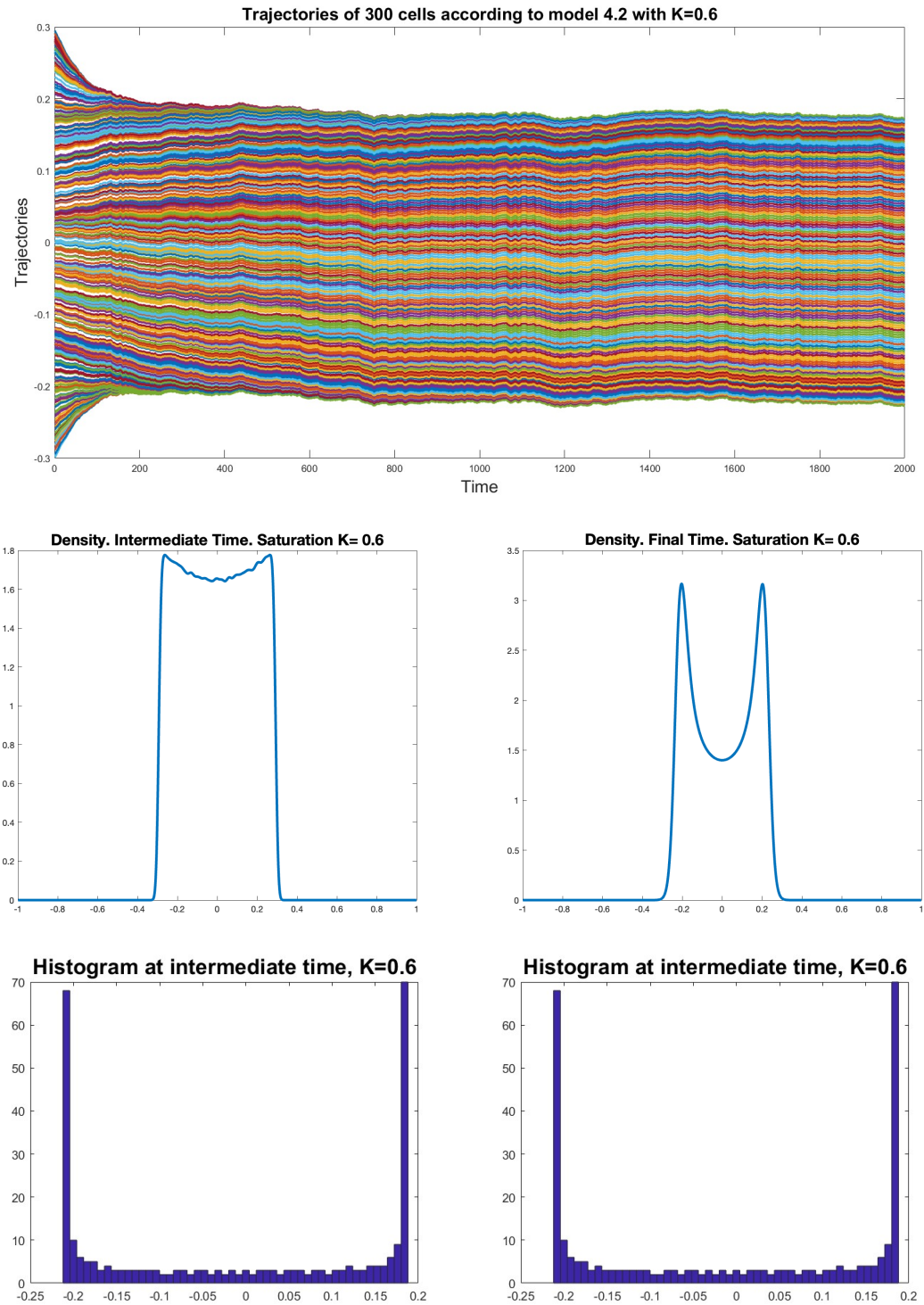


FIGURE 16. Nonlocal saturation model,  $K = 0.6$ , Concentrated initial data within  $[-0.3, 0.3]$ . First row trajectories with  $N = 300$  cells, second row densities of the PDE model (§3.5.3) and third one histograms of SDEs (§4.2). Both at intermediate time on the left and at final time on the right.

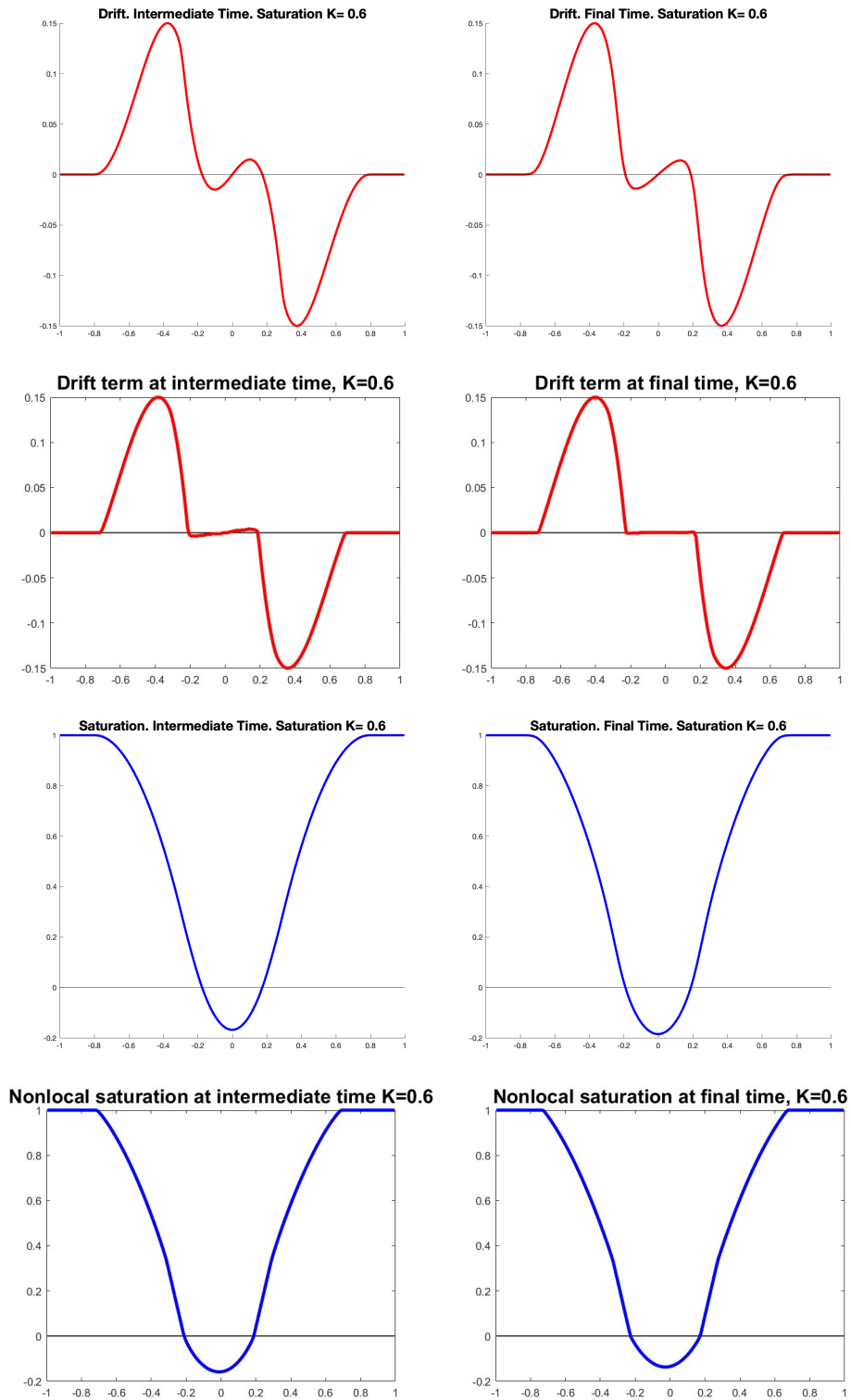


FIGURE 17. Drifts and saturations for nonlocal saturation model,  $K = 0.6$ , Concentrated initial data within  $[-0.3, 0.3]$ . Drifts in first and second rows for PDE model (§3.5.3) and SDEs (§4.2), respectively. Saturations in third and fourth rows for PDE model (§3.5.3) and SDEs (§4.2), respectively. All of them at intermediate time on the left and at final time on the right.

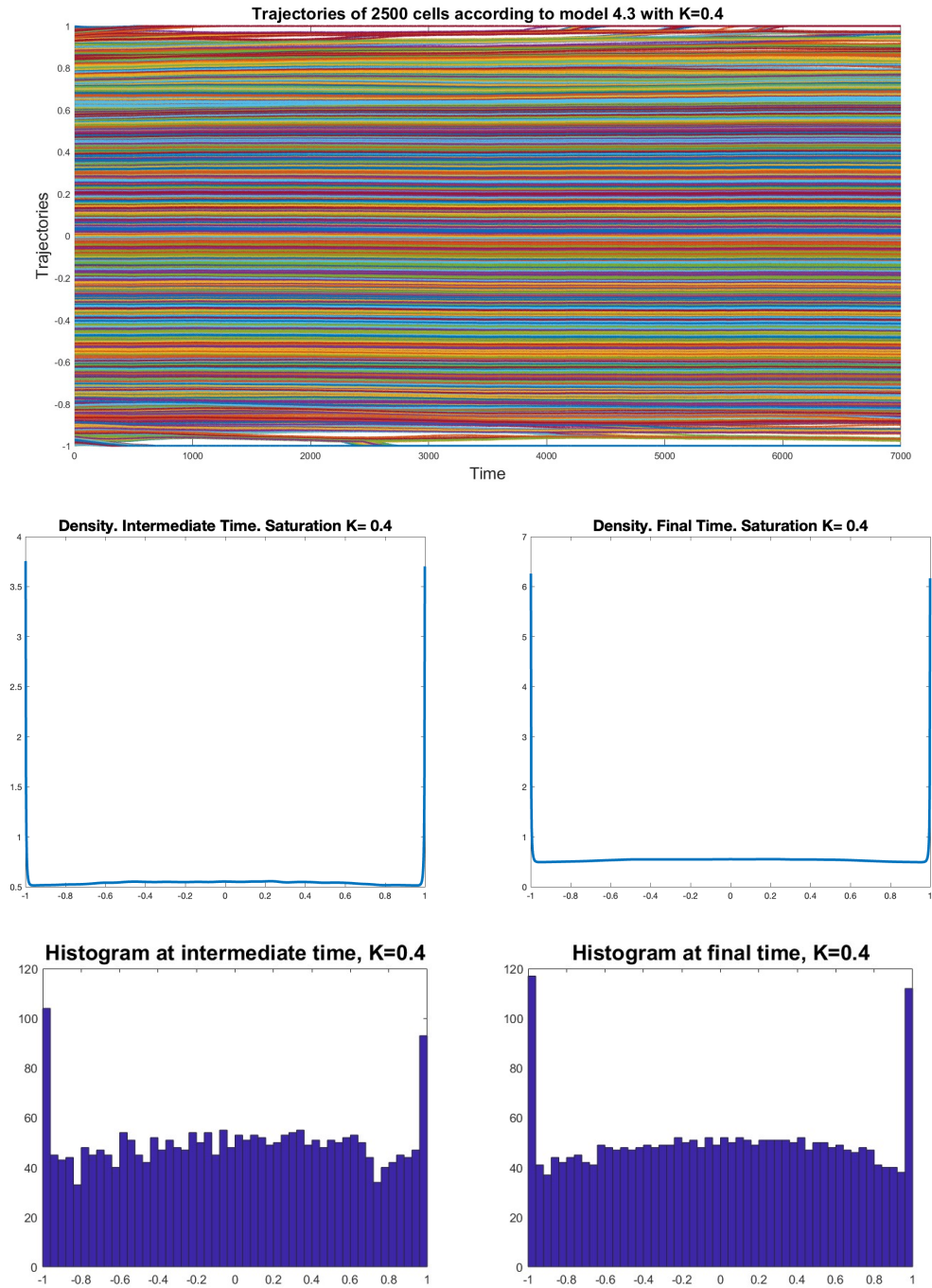
5.4. Intermediate repulsion  $K = 0.4$ .

FIGURE 18. Local saturation model,  $K = 0.4$ . First row trajectories with  $N = 2500$  cells, second row densities of the PDE model (§3.5.2) and third one histograms of SDEs (§4.3). Both at intermediate time on the left and at final time on the right.

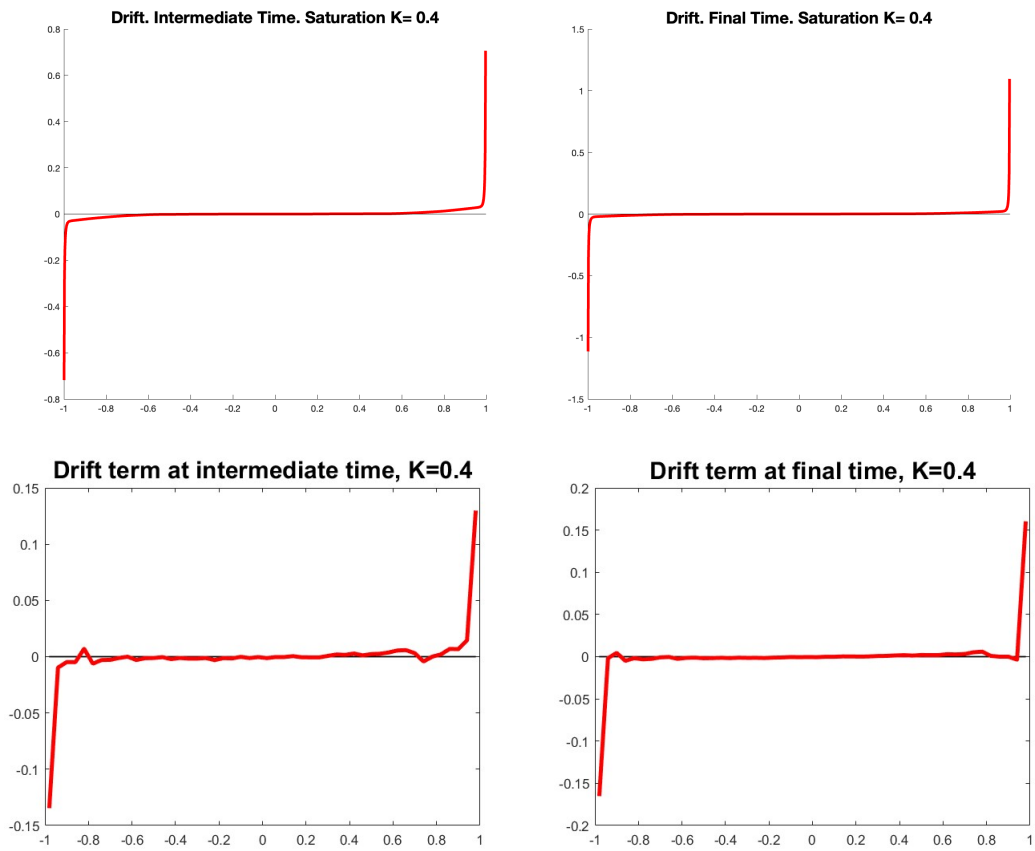


FIGURE 19. Drifts for local saturation model,  $K = 0.4$ . First row PDE model (§3.5.2) and second row SDEs (§4.3). Both at intermediate time on the left and at final time on the right.

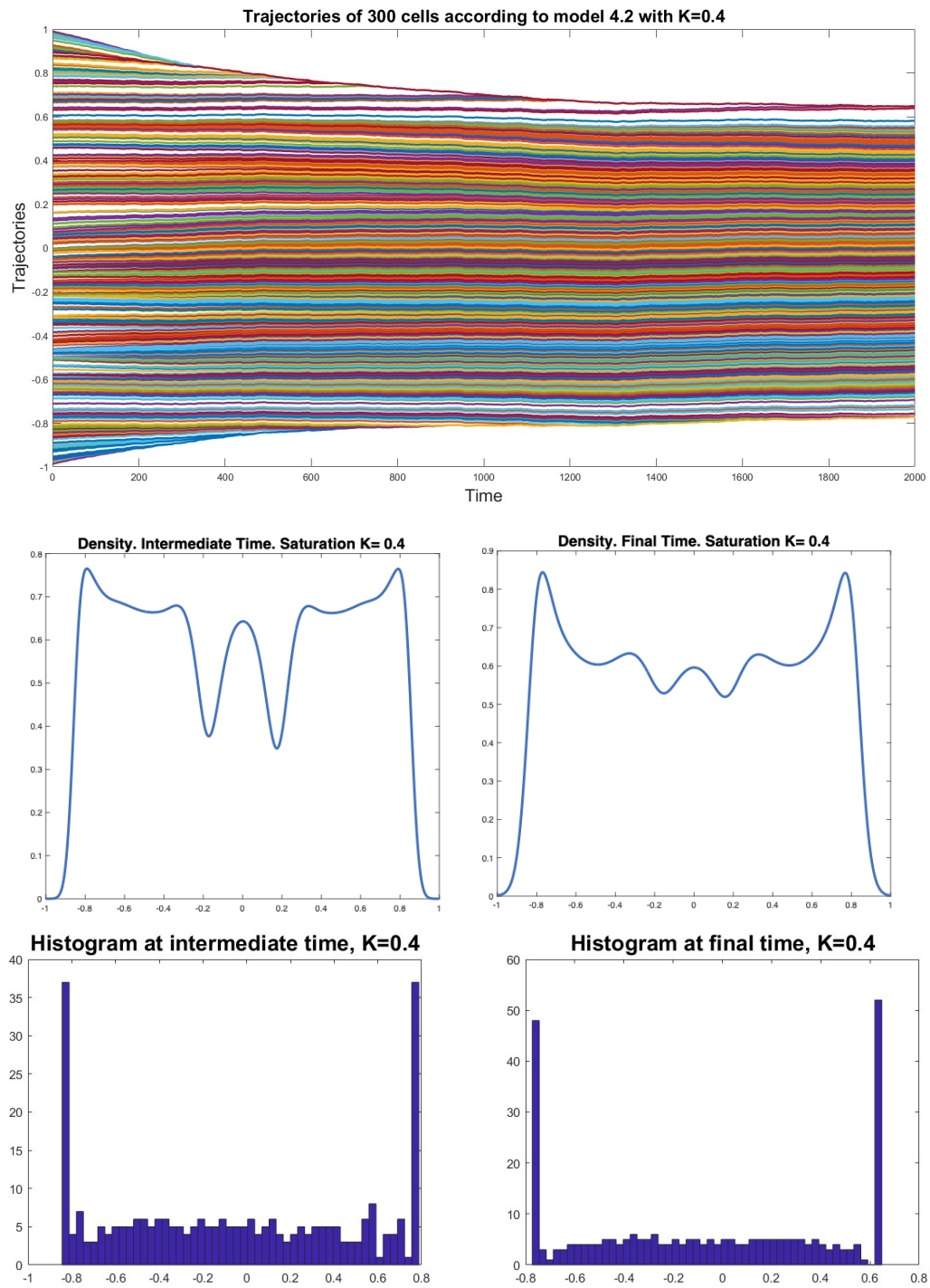


FIGURE 20. Nonlocal saturation model,  $K = 0.4$ . First row trajectories with  $N = 300$  cells, second row densities of the PDE model (§3.5.3) and third one histograms of SDEs (§4.2). Both at intermediate time on the left and at final time on the right.

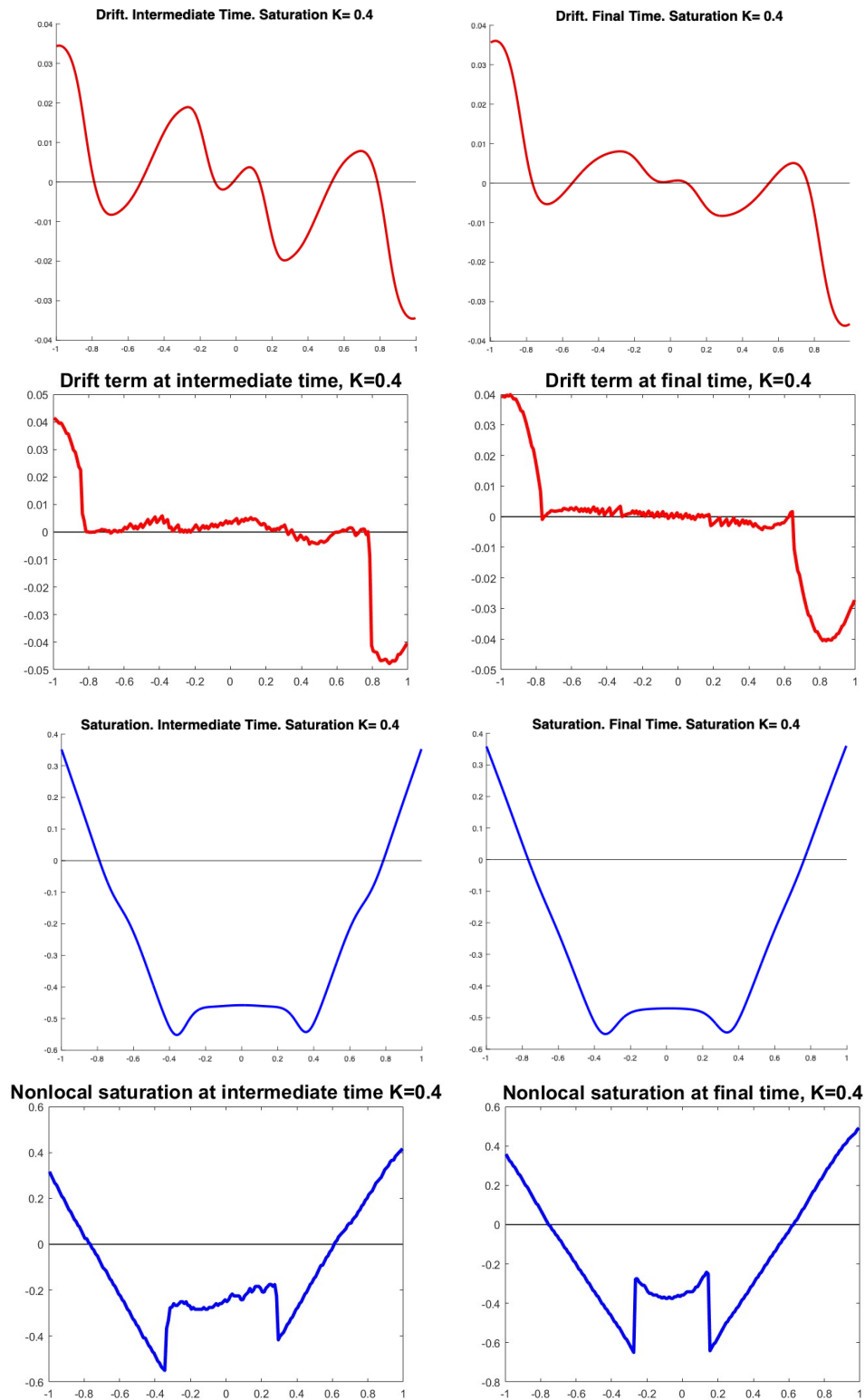


FIGURE 21. Drifts and saturations for nonlocal saturation model,  $K = 0.4$ . Drifts in first and second rows for PDE model (§3.5.3) and SDEs (§4.2), respectively. Saturations in third and fourth rows for PDE model (§3.5.3) and SDEs (§4.2), respectively. All of them at intermediate time on the left and at final time on the right.

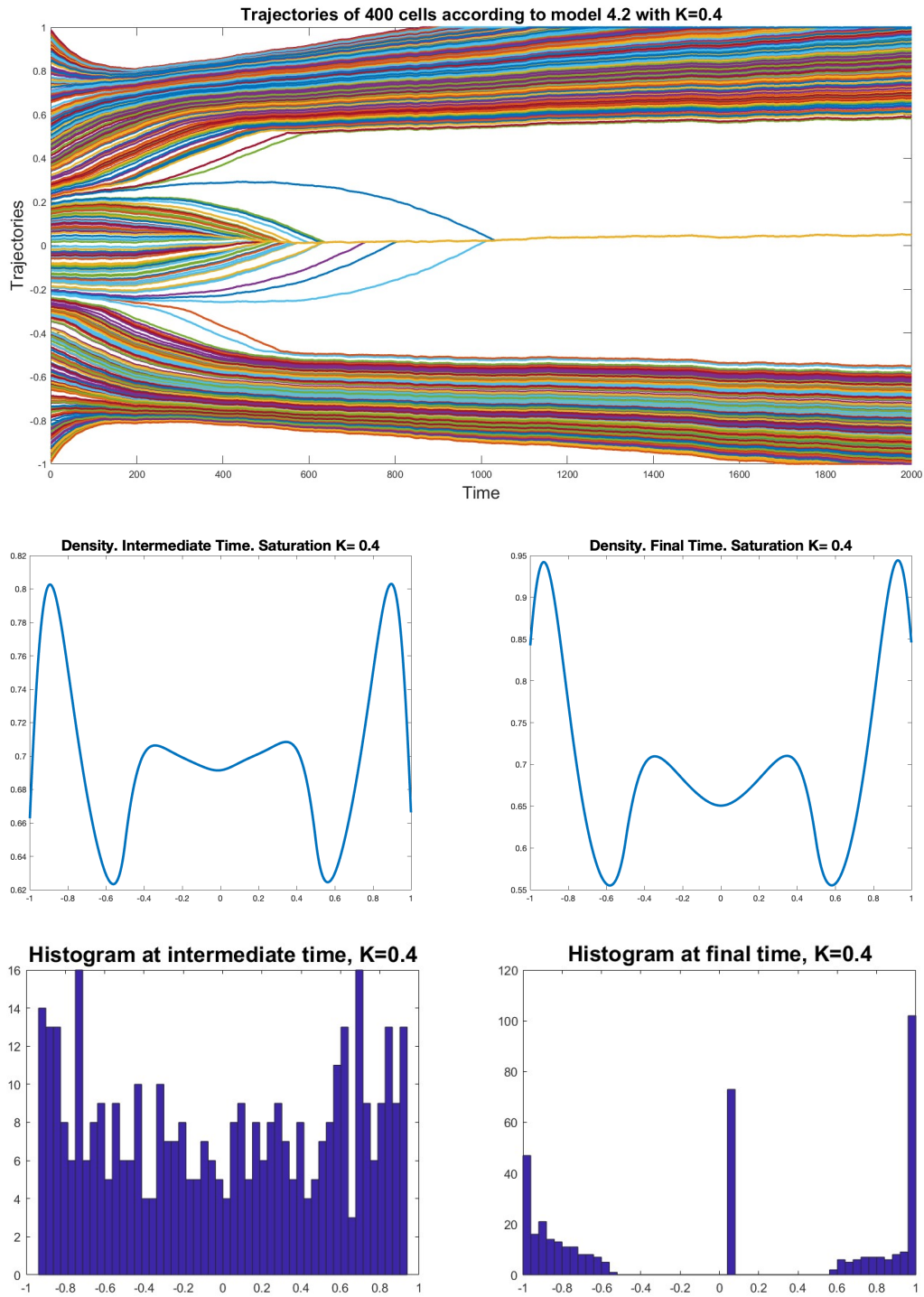


FIGURE 22. Nonlocal saturation model,  $K = 0.4$  and constant weight. First row trajectories with  $N = 300$  cells, second row densities of the PDE model (§3.5.3) and third one histograms of SDEs (§4.2). Both at intermediate time on the left and at final time on the right.

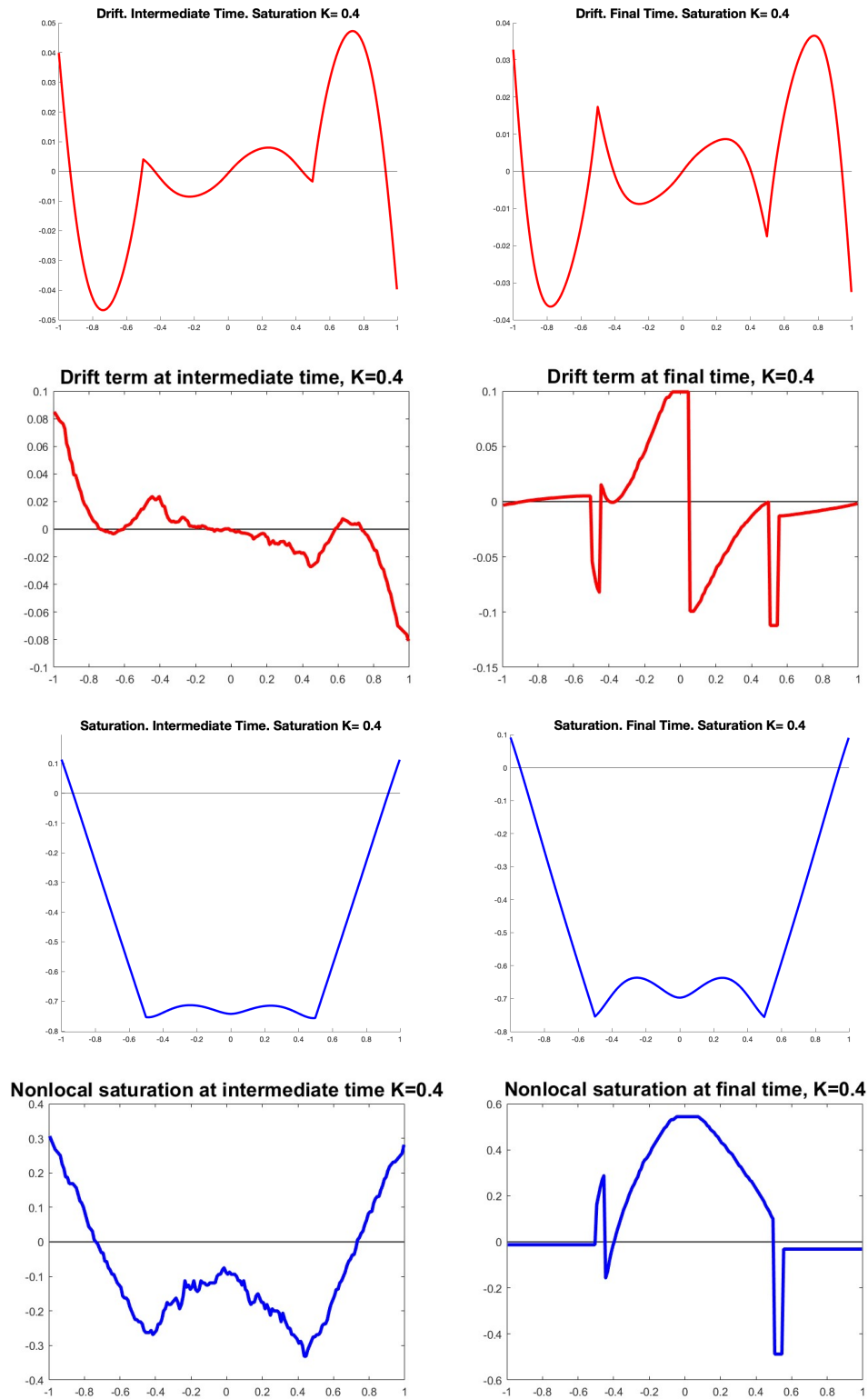


FIGURE 23. Drifts and saturations for nonlocal saturation model,  $K = 0.4$  and constant weight. Drifts in first and second rows for PDE model (§3.5.3) and SDEs (§4.2), respectively. Saturations in third and fourth rows for PDE model (§3.5.3) and SDEs (§4.2), respectively. All of them at intermediate time on the left and at final time on the right.

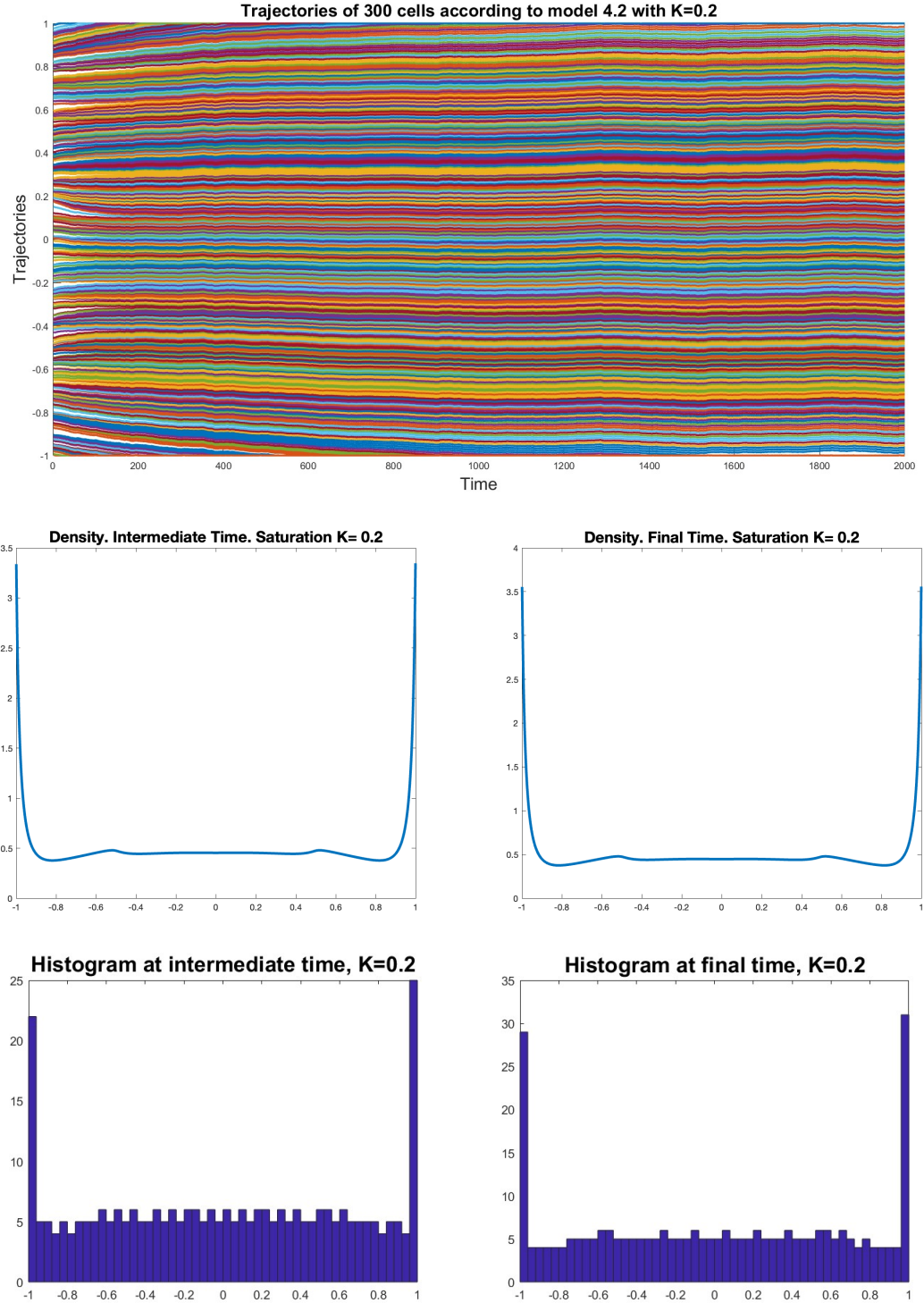
5.5. Strong repulsion  $K = 0.2$ .

FIGURE 24. Nonlocal saturation model,  $K = 0.2$ . First row trajectories with  $N = 300$  cells, second row densities of the PDE model (§3.5.3) and third one histograms of SDEs (§4.2). Both at intermediate time on the left and at final time on the right.

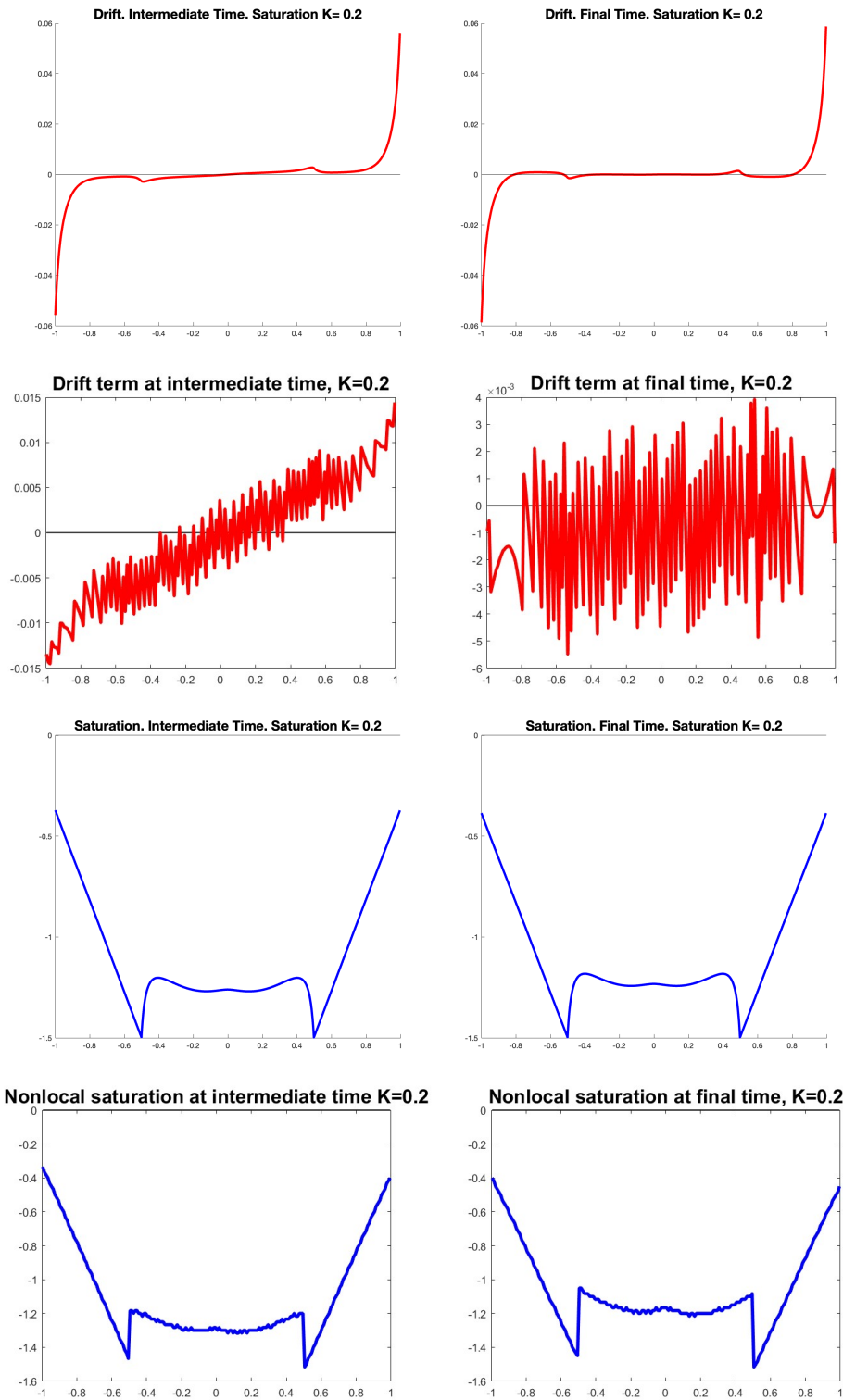


FIGURE 25. Drifts and saturations for nonlocal saturation model,  $K = 0.2$ . Drifts in first and second rows for PDE model (§3.5.3) and SDEs (§4.2), respectively. Saturations in third and fourth rows for PDE model (§3.5.3) and SDEs (§4.2), respectively. All of them at intermediate time on the left and at final time on the right.

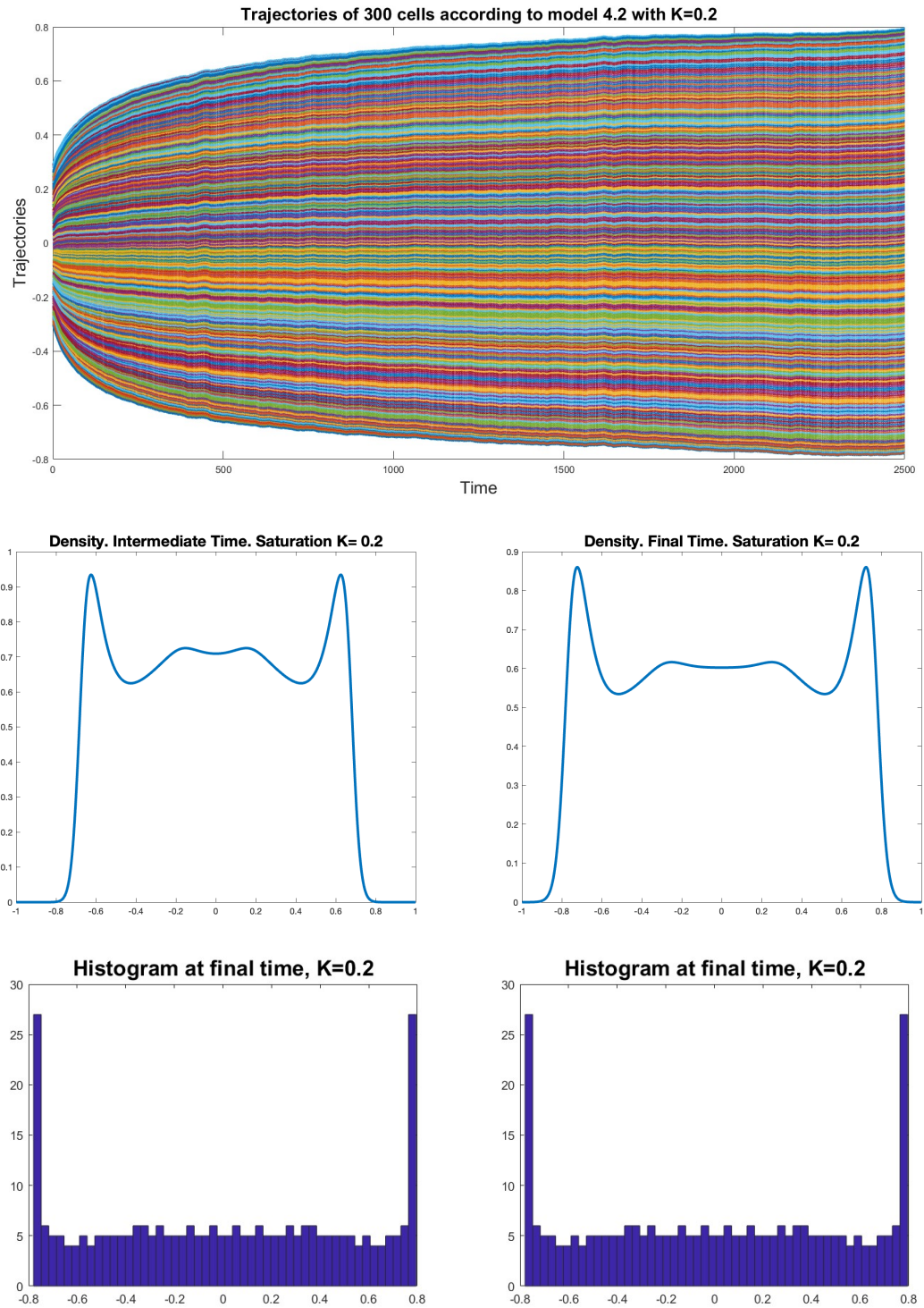


FIGURE 26. Nonlocal saturation model,  $K = 0.2$ , Concentrated initial data within  $[-0.3, 0.3]$ . First row trajectories with  $N = 300$  cells, second row densities of the PDE model (§3.5.3) and third one histograms of SDEs (§4.2). Both at intermediate time on the left and at final time on the right.

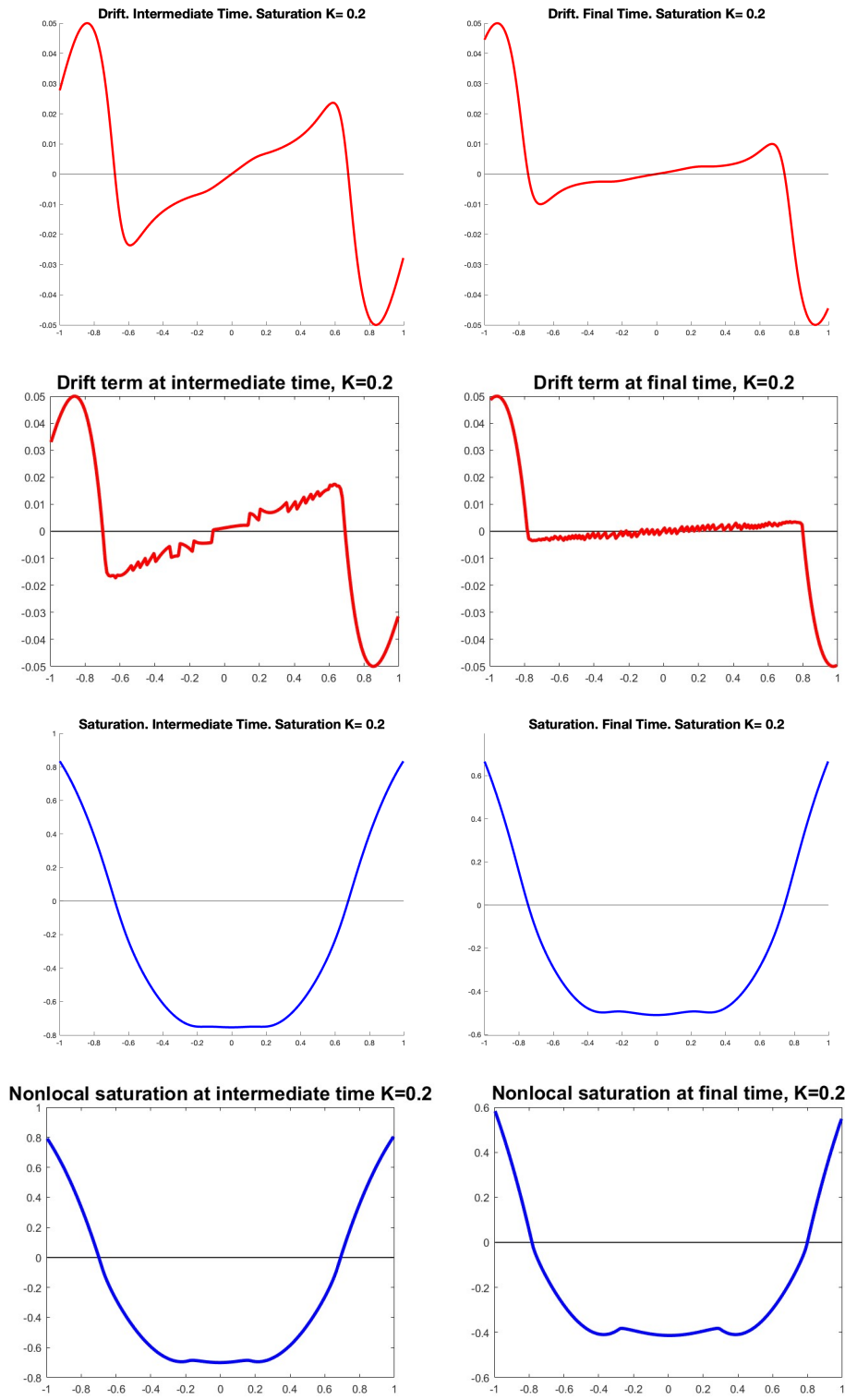


FIGURE 27. Drifts and saturations for nonlocal saturation model,  $K = 0.2$ , Concentrated initial data within  $[-0.3, 0.3]$ . Drifts in first and second rows for PDE model (§3.5.3) and SDEs (§4.2), respectively. Saturations in third and fourth rows for PDE model (§3.5.3) and SDEs (§4.2), respectively. All of them at intermediate time on the left and at final time on the right.

## 6. CONCLUSIONS AND PERSPECTIVES

In this work we propose two different discrete approaches to approximate cell-cell adhesion models. On the one hand, from Eulerian perspective as a balance of gain and loss terms deduced in Section 3, on the other hand following particles trajectories in Section 4. In both cases, they describe identical dynamics when applied to the specific models: APS in [2] and the local saturation model studied in [12], but considering homogeneous boundary conditions, instead of periodic boundary conditions as in the mentioned papers.

In addition, we also introduce a new cell-cell adhesion model, accounting for saturation effects by multiplying the drift term by a nonlocal coefficient. Eulerian and Lagrangian approach also show similar dynamics. However, the behaviour of the solutions obeying nonlocal saturation effect clearly differs with respect to the models in [2] and [12]. Indeed, our model is suitable to describe very different dynamics: it is capable to disseminate the cells along the whole domain, as well as it can recover high aggregation peaks as in the APS model, passing by intermediate scenarios of moderate aggregation, just varying the values of  $K$  and the weight  $w$ .

Moreover, our model includes saturation or even repulsion from too crowded areas as part of the interaction terms, in contrast to [12] where this repulsion is driven by a porous media type diffusion.

As a continuation of this work, we wish to model cell motion due to external cues, that could modify their natural trajectories. The action of certain signals or irregularities in the media could drive the cells to prescribed areas and produce long range motion. Some nonlocal operators can diffuse the particles in these anisotropic or prescribed way, instead of arranging them averaged, and produce nonlocal jumps. This anisotropic long range diffusion would compete with the interaction drift term, that should also accounts for saturation or repulsion from too populated areas.

**Acknowledgements:** This research was initially conducted while CGF visited University of Seville thanks to the Feder project entitled *Diferentes Perspectivas para Modelos Biomatemáticos: Modelización, Análisis y Aproximación* (US-1381261). At present FGG and MPL are supported by project PID2023-149182NB-I00, and AS is supported by project PID2023-149509NB-I00. The authors wish to thank deeply to both referees for their numerous and valuable comments and suggestions, which improved unquestionably the content and presentation of a previous version of the manuscript.

## REFERENCES

1. K. Anguige and C. Schmeiser, *A one-dimensional model of cell diffusion and aggregation, incorporating volume filling and cell-to-cell adhesion*, J. Math. Biol. **58** (2009), no. 3, 395–427. MR 2470195
2. N. J. Armstrong, K. J. Painter, and J. A. Sherratt, *A continuum approach to modelling cell-cell adhesion*, J. Theoret. Biol. **243** (2006), no. 1, 98–113.
3. N. Bellomo and M. Pulvirenti, *Generalized kinetic models in applied sciences*, Modeling in applied sciences, Model. Simul. Sci. Eng. Technol., Birkhäuser Boston, Boston, MA, 2000, pp. 1–19. MR 1763150
4. Howard C. Berg, *Random walks in biology*, Princeton University Press, Princeton, NJ, 1983. MR 835706
5. F. Bolley, *Limite de champ moyen de systèmes de particules*, Séminaire: Equations aux Dérivées Partielles. 2009–2010, Sémin. Équ. Dériv. Partielles, École Polytech., Palaiseau, 2012, pp. Exp. No. XXXI, 15. MR 3098635
6. P.C. Bressloff, *Stochastic processes in cell biology*, Interdisciplinary Applied Mathematics, vol. 41, Springer, Cham, 2014. MR 3244328
7. A. Buttenschön and T. Hillen, *Non-local cell adhesion models: Symmetries and bifurcations in 1-d*, Springer, New York., 2021.
8. V. Capasso and D. Bakstein, *An introduction to continuous-time stochastic processes*, third ed., Modeling and Simulation in Science, Engineering and Technology, Birkhäuser/Springer, New York, 2015, Theory, models, and applications to finance, biology, and medicine. MR 3362672

9. J. A. Carrillo, K. Craig, and Y. Yao, *Aggregation-diffusion equations: dynamics, asymptotics, and singular limits*, Active particles. Vol. 2. Advances in theory, models, and applications, Model. Simul. Sci. Eng. Technol., Birkhäuser/Springer, Cham, 2019, pp. 65–108. MR 3932458
10. J. A. Carrillo, R. Eftimie, and F. Hoffmann, *Non-local kinetic and macroscopic models for self-organised animal aggregations*, Kinet. Relat. Models **8** (2015), no. 3, 413–441. MR 3404767
11. J. A. Carrillo, M. Fornasier, G. Toscani, and F. Vecil, *Particle, kinetic, and hydrodynamic models of swarming*, Mathematical modeling of collective behavior in socio-economic and life sciences, Model. Simul. Sci. Eng. Technol., Birkhäuser Boston, Boston, MA, 2010, pp. 297–336. MR 2744704
12. J. A. Carrillo, H. Murakawa, M. Sato, H. Togashi, and O. Trush, *A population dynamics model of cell-cell adhesion incorporating population pressure and density saturation*, J. Theoret. Biol. **474** (2019), 14–24. MR 3948738
13. L. Chen, K. Painter, C. Surulescu, and A. Zhigun, *Mathematical models for cell migration: a non-local perspective*, Philosophical Transactions of the Royal Society B: Biological Sciences **375** (2020), no. 1807, 20190379.
14. J. M. Coron, A. Keimer, and L. Pflug, *Nonlocal transport equations: existence and uniqueness of solutions and relation to the corresponding conservation laws*, SIAM J. Math. Anal. **52** (2020), no. 6, 5500–5532. MR 4172728
15. F. Cucker and S. Smale, *Emergent behavior in flocks*, IEEE Trans. Automat. Control **52** (2007), no. 5, 852–862. MR 2324245
16. M. Di Francesco, S. Fagioli, and E. Radici, *Deterministic particle approximation for nonlocal transport equations with nonlinear mobility*, J. Differential Equations **266** (2019), no. 5, 2830–2868. MR 3906267
17. V. Giunta, T. Hillen, M. Lewis, and J. R. Potts, *Local and global existence for nonlocal multispecies advection-diffusion models*, SIAM J. Appl. Dyn. Syst. **21** (2022), no. 3, 1686–1708. MR 4447423
18. T. Hillen and A. Buttenschön, *Nonlocal adhesion models for microorganisms on bounded domains*, SIAM J. Appl. Math. **80** (2020), no. 1, 382–401. MR 4062808
19. T. Hillen, K. Painter, and C. Schmeiser, *Global existence for chemotaxis with finite sampling radius*, Discrete Contin. Dyn. Syst. Ser. B **7** (2007), no. 1, 125–144. MR 2257455
20. A. Colombi, J. A. Carrillo and M. Scianna, *Adhesion and volume constraints via nonlocal interactions determine cell organisation and migration profiles*, J. Theoret. Biol. **445** (2018), 75–91. MR 3772722
21. N. I. Kavallaris and T. Suzuki, *Non-local partial differential equations for engineering and biology*, Mathematics for Industry (Tokyo), vol. 31, Springer, Cham, 2018, Mathematical modeling and analysis. MR 3752137
22. T. Hillen, K. J. Painter and Jonathan J. R. Potts, *Biological modeling with nonlocal advection-diffusion equations*, Math. Models Methods Appl. Sci. **34** (2024), no. 1, 57–107. MR 4683281
23. H. Levine, W. J. Rappel, and I. Cohen, *Self-organization in systems of self-propelled particles*, Phys. Rev. E **63** (2000), 017101.
24. A. Mogilner and L. Edelstein-Keshet, *A non-local model for a swarm*, J. Math. Biol. **38** (1999), no. 6, 534–570. MR 1698215
25. H. Murakawa and H. Togashi, *Continuous models for cell-cell adhesion*, J. Theoret. Biol. **374** (2015), 1–12.
26. K. J. Painter, J. M. Bloomfield, J. A. Sherratt, and A. Gerisch, *A nonlocal model for contact attraction and repulsion in heterogeneous cell populations*, Bull. Math. Biol. **77** (2015), no. 6, 1132–1165. MR 3357726
27. J. P. Pinasco, V. Semeshenko, and P. Balenzuela, *Modeling opinion dynamics: theoretical analysis and continuous approximation*, Chaos Solitons Fractals **98** (2017), 210–215. MR 3632850
28. N. Saito, *Conservative upwind finite-element method for a simplified Keller-Segel system modelling chemotaxis*, IMA J. Numer. Anal. **27** (2007), no. 2, 332–365. MR 2317007
29. K. J. Painter, T. Hillen and M. Winkler, *Global solvability and explicit bounds for non-local adhesion models*, European J. Appl. Math. **29** (2018), no. 4, 645–684. MR 3819991
30. J. M. Teddy and P. M. Kulesa, *In vivo evidence for short- and long-range cell communication in cranial neural crest cells*, Development **131** (2004), no. 24, 6141–6151.
31. C. M. Topaz, A. L. Bertozzi, and M. A. Lewis, *A nonlocal continuum model for biological aggregation*, Bull. Math. Biol. **68** (2006), no. 7, 1601–1623. MR 2257718

CARLO GIAMBIAGI FERRARI, FRANCISCO GUILLÉN-GONZÁLEZ, MAYTE PÉREZ-LLANOS AND ANTONIO SUÁREZ  
 DEPARTAMENTO DE ECUACIONES DIFERENCIALES Y ANÁLISIS NUMÉRICO  
 FACULTAD DE MATEMÁTICAS, U. DE SEVILLA, C. TÁRFA, s/n, 41012 SEVILLA, SPAIN  
 Email address: cgf@gmail.com, guillen@us.es, mpperez@us.es, suarez@us.es